

BeppoSAX-WFC catalog of fast X-ray transients

J.J.M. in 't Zand¹, C. Guidorzi^{2,3}, J. Heise¹, L. Amati³, E. Kuulkers⁴, F. Frontera^{2,3}, G. Gianfagna⁵, and L. Piro⁵

¹ SRON Space Research Organization Netherlands, Niels Bohrweg 4, 2333 CA Leiden, the Netherlands

² Dept. of Physics and Earth Science, University of Ferrara, 44122 Ferrara, Italy

³ INAF-OAS Bologna, Via P. Gobetti 101, 40129, Bologna, Italy

⁴ ESTEC, ESA, Keplerlaan 1, 2201 AZ Noordwijk, the Netherlands

⁵ INAF-IAPS Roma, via Fosso del Cavaliere 100, 00133 Rome, Italy

Submitted to A&A on December 18, 2025

ABSTRACT

We performed a search for fast X-ray transients (FXTs), with durations longer than one second and less than one day, through data of the Wide Field Camera (WFC) instrument onboard the BeppoSAX X-ray observatory collected between June 1996 and April 2002. The WFC sensitivity ranged from 10^{-9} erg s $^{-1}$ cm $^{-2}$ (2-10 keV), for a time scale of 10 s, to a few times 10^{-11} erg s $^{-1}$ cm $^{-2}$ for a time scale of 10^5 s. We focused our search on gamma-ray bursts (GRBs), X-ray flashes (XRFs), X-ray flares from high-mass X-ray binaries and stellar flares, while Type-I and II X-ray bursts from Galactic neutron stars were excluded. 149 such fast transient events were detected. 63 of these are new to the literature. 38 flares are identified with 22 nearby stars. Three stars have never been seen flaring before in X-rays or optical (NLTT 51688, GR Dra and UCAC4 255-003783). We find that the MeV transient GRO J1753+57 is most likely the same object as GR Dra rather than an AGN as previously thought. Eleven flares were detected from known high-mass X-ray binaries with irregular wind accretion (four of which are of the subclass of supergiant fast X-ray transients). 100 GRBs were identified of which 24 have not been published before. We classify 37% of the X-ray detected GRBs as XRFs with relatively large X-ray to gamma-ray flux ratio, gamma-rays being measured with the BeppoSAX Gamma Ray Burst Monitor. The duration/spectral hardness distribution of all FXTs is bimodal, separating the group roughly in transients shorter and longer than 1 ksec and with relatively hard and soft spectra, respectively. We identify the 'short' FXTs as GRBs and XRFs and the 'long' FXTs as flares from nearby late-type stars and X-ray binaries. The BeppoSAX-WFC FXT sample is found to be consistent with the one observed by Einstein Probe, when the sensitivity of the two instruments is taken into account.

Key words. Catalogs – Gamma-ray bursts – Gamma-rays: stars – X-rays: bursts – X-rays: binaries – Stars: flare

1. Introduction

The X-ray sky is dynamic, more so than the visual sky. Variability is detected on all observable time scales and up to the largest amplitudes. Often the dynamical range is so large that sources change from undetectable to the brightest levels and back. This we call a transient event. The duration of this transient activity can vary between milliseconds (e.g., soft gamma-ray repeaters and type-II bursts) to years (e.g., low-mass X-ray binaries). One class of transients concerns those that last shorter than 1 day and longer than 1 s and are generally not associated with the X-ray bright accreting compact objects in X-ray binaries. Such transients are generically called fast X-ray transients (FXTs), but they include a mixture of different sources.

The brightest FXTs are Gamma Ray Bursts (GRBs) and stellar flares. GRBs happen in external galaxies and are associated with two different classes of progenitors, where the collapse of a massive star or the merging two compact objects (neutron stars, black holes) yields a relativistic expanding jet that produces the GRB and its afterglow (e.g., review by Kumar & Zhang 2015). Stellar flares are abundant in stars of spectral type of the Sun and later, and young T Tau stars. This was convincingly shown by Kepler and TESS, the latter of which detected more than 120 thousand of them in the optical (e.g., Seli et al. 2025). TESS detected stellar flares in 7.5% of all monitored stars. The X-ray counterparts to stellar flares have peak luminosities of 10^{28} - 10^{31} erg s $^{-1}$ (Pye et al. 2015), except for 'superflares' that can

be up to 10^3 times more luminous. For typical sensitivities of about 10^{-10} erg s $^{-1}$ cm $^{-2}$, these flares can be detected up to a few hundred parsecs distance, which renders them an isotropic sky distribution just like the extragalactic GRBs.

FXTs have been detected ever since the advent of space-borne X-ray astronomy. Two early reports are Heise et al. (1975) and Rappaport et al. (1976). The first systematic studies on complete databases of some X-ray instruments were published in the 1980s. Connors et al. (1986) study data taken by the HEAO 1 A-2 experiment in the 2 to 60 keV bandpass at a sensitivity of 10^{-10} erg s $^{-1}$ cm $^{-2}$ (on a time scale of a few seconds) and discovered five transients with durations of 60 to 2000 s and peak fluxes up to 10^{-9} erg s $^{-1}$ cm $^{-2}$. The rate corresponds to $10^{4.2} \times 10^5$ such transients per year over the whole sky, or 10-200 above a threshold of 10^{-8} erg s $^{-1}$ cm $^{-2}$. Connors et al. suggested that most events are stellar flares from dMe-dKe stars, caused similarly as solar flares, namely by magnetic reconnection events.

Ambruster & Wood (1986) reports ten transients with the HEAO 1 A-1 experiment, eight of which are stellar flares and two are speculated to be X-ray counterparts to faint GRBs. They infer an all-sky rate of 1500-3000 yr $^{-1}$ above 8×10^{-11} erg s $^{-1}$ cm $^{-2}$ (0.5-20 keV).

Pye & McHardy (1983) reports twenty-seven hours-long transients with Ariel-V SSI, eleven of which are identified with stellar flares and one is associated with a GRB. The remaining transients are speculated to be a mix of these types of

sources. The all-sky rate is inferred to be $\sim 1500 \text{ yr}^{-1}$ above $4 \times 10^{-10} \text{ erg s}^{-1} \text{cm}^{-2}$ (2-18 keV).

Gotthelf et al. (1996) search through all IPC (Imaging Proportional Counter) data in the 0.5-3.5 keV bandpass from the Einstein Observatory for transients lasting shorter than 10 s and find 42 cases with peak fluxes between 2×10^{-10} and $1 \times 10^{-9} \text{ erg s}^{-1} \text{cm}^{-2}$. This implies an all-sky rate of $2 \times 10^6 \text{ yr}^{-1}$ or 16 yr^{-1} above $1 \times 10^{-8} \text{ erg s}^{-1} \text{cm}^{-2}$ which appears comparable with the Connors et al. result although there is a narrower selection for duration.

Arefiev et al. (2003) combines data sets, investigating a 'few hundred' FXTs from six instruments on five observatories that operated in the 1970s through 1990s with widely different sensitivities and fields of view. They conclude that FXTs comprise a variety of types of sources, predominantly GRBs and stellar flares and that the origin of many, particularly apparent GRBs without gamma-ray signals, are of unknown origin. Arefiev et al. estimate an all-sky rate of tens of thousands per year above a fluence of 10^{-2} Crab-sec.

Searches of FXTs at much fainter fluxes than mentioned above were also carried out with X-ray narrow field telescopes aboard XMM, Chandra, ROSAT, XISM (e.g., Sun et al. 1998; Quirola-Vásquez et al. 2022; Tsuboi et al. 2024). Several faint FXTs with duration from about 100 s to 1000 s were found down to flux of around $10^{-13} \text{ erg s}^{-1} \text{cm}^{-2}$. In this regime, a wider variety of sources are making up FXTs. In addition to stellar flares and GRBs (with and without gamma-ray emission) that are dominating the brighter end, faint FXT include tidal disruption events, supernova shock break out, GRBs orphan afterglows and quasi-periodic eruptions from massive black holes.

Currently, there are two work horses for detecting FXTs with wide field monitors: MAXI (Monitoring of All-sky X-ray Image) on the International Space Station (Matsuoka et al. 2009) and WXT (Wide-field X-ray Telescope) on the Einstein Probe (EP, Yuan et al. 2022, 2025). MAXI is particularly efficient in detecting stellar flares since those generally last longer than the sample time of any point on the sky of about 1 min per 1.5 hr. MAXI has for the past 15 years (up to October 10, 2025) reported through its alert messaging system 150 stellar flares from 29 sources (e.g., Tsuboi & Sasaki 2020). WXT is perfectly suited for detecting FXTs, thanks to its large instantaneous field of view of 3600 square degrees and its deep sensitivity of $2.6 \times 10^{-11} \text{ erg s}^{-1} \text{cm}^{-2}$ (0.8 mCrab) in a 1000 s observation in soft X-rays (0.5-4 keV). A preliminary analysis of the first year of EP observations (Wu et al. 2025) resulted in 128 transients, that included 28 stellar flares, 30 events with a gamma-ray counterpart and 52 events without. Another study (Zhang et al. 2025b) searched the gamma-ray counterpart in 63 FXTs detected by EP (that excluded stellar flares and known sources), finding 14 such events. While the identification of the full EP sample is ongoing, extensive follow-up observations of a subset shows that several of them are associated to GRBs, including high redshift GRBs, XRFs (e.g., Liu et al. 2025; Gianfagna et al. 2025; Sun et al. 2025) but also some to TDE (Li et al. 2025) and odd-balls (Zhang et al. 2025a).

In the 1980s, FXTs were ill understood and in strong need of exploration. Thanks to the prospering development of wide-field coded aperture cameras with large-area multiwire proportional counters (e.g., Proctor et al. 1978; Fenimore & Cannon 1978; Willmore et al. 1984; Brinkman et al. 1985; Skinner et al. 1987; Mels et al. 1988), SRON started in the mid-1980s the successful design and construction of the Wide Field Camera (WFC) instrument for the Italian-Dutch BeppoSAX X-ray observatory with the specific goal to collect data on FXTs. The WFC was launched

in April 1996. The mission lasted 6 years. The WFC was very successful in detecting thousands of transient events and, for instance, made an essential contribution to solving the GRB distance scale (Costa et al. 1997b; van Paradijs et al. 1997). Much work with the WFC has been published, but a specific paper reporting the complete results of the FXTs detected by the WFC and their proposed identification has been missing. The present paper is particularly important because it provides a complete flux-limited sample of FXTs, providing a reference also for current wide field monitor missions.

We have performed a systematic search of FXTs in the WFC data archive, which, thanks to enormously improved computational capabilities in the two decades since the operational end, has become much easier. In addition, we provide simultaneous data from the Gamma-Ray Burst Monitor (GRBM) on BeppoSAX, enabling for all these WFC FXTs a homogenous coverage of their gamma-ray emission. We further supplement their gamma-ray properties with data from the Burst And Transient Source Experiment (BATSE) on the Compton Gamma-Ray Observatory when available. We present some analyses of the catalog and compare them with previous studies from other satellites. In Sect. 2, we describe the employed instrumentation, in Sect. 3 the observations and in Sect. 4 the method of search for FXTs in WFC data. The result is a catalog that is described in Sect. 5. Section 6 discusses the analysis of the overall spectra and classification of the uncertain cases in the catalog. Section 7 presents a discussion of the results.

2. Instrumental description

BeppoSAX (Boella et al. 1997) hosted two identical cameras comprising the WFC (Jager et al. 1997), pointed in opposite directions and perpendicular to the pointing of the three narrow field instruments (NFI) onboard (LECS, MECS, PDS). They were coded aperture cameras, consisting of a multi-wire position sensitive large-area ($25.6 \times 25.6 \text{ cm}^2$) proportional counter (Mels et al. 1988) paired with, at a distance of 70 cm, a similarly sized gold-plated stainless-steel mask etched with 20 thousand holes following a pattern based on a triadic difference set (in 't Zand et al. 1994). This resulted in the following characteristics: a bandpass of 2 to 30 keV, a photon energy resolution of 20% at 6 keV (full width at half maximum), a net effective area of 141 cm^2 at 6 keV, a highest possible photon detection rate of 2000 s^{-1} , a field of view 40×40 square degrees (3.7% sky coverage per camera), an angular resolution of 5 arcmin and a source location accuracy down to 0.7 arcmin (99% confidence). As a reference, the standard Crab X-ray source, when placed on axis, had a photon-count rate of 280 s^{-1} in the full bandpass, while the count rate due to the cosmic diffuse X-ray background was approximately 160 s^{-1} .

The coded aperture yields coded detector images that need to be decoded on the ground to obtain sky images. This imaging has the advantage, compared to focusing techniques, that it enables a large field of view and relatively cheap optics, but the disadvantage is that photons of all celestial sources are detected on the same detector area resulting in cross talk between different positions in the field of view. The WFC sensitivity ranged between 15 mCrab (2-30 keV, integration time 1000 s) in the crowded Galactic center field with many bright sources, particularly Sco X-1, and 6 mCrab far away from the Galactic plane (5-sigma detection threshold). An in-depth description of the WFC can be found in Jager et al. (1997).

The WFC instrument was very well suited for detecting FXTs because they combined roughly 1-day exposures with a

large field of view at sufficiently high angular resolution to enable identification with known X-ray sources or counterparts in the optical, radio or other wavelengths.

The second instrument on board BeppoSAX relevant for the present study is the GRBM (Amati et al. 1997; Feroci et al. 1997; Costa et al. 1998). It consisted of the four lateral shields of the Phoswich Detector System (Frontera et al. 1997), each with a size of 1136 cm^2 , had a bandpass of 40 to 700 keV and a sensitivity of $10^{-8} \text{ erg s}^{-1} \text{ cm}^{-2}$ for 1 s. Two shields were perpendicular to the viewing direction of a WFC unit. Therefore, an event observed with a WFC camera had an optimum GRBM collecting area.

Finally, we use publicly available data¹ from the BATSE instrument (Fishman et al. 1994; Paciesas et al. 1999) on the Compton Gamma-Ray Observatory (CGRO). This was an array of NaI detectors for the study of GRBs that flew from 1991 to 2000 and had full sky coverage in the nominal 20-325 keV bandpass.

3. Observations

The BeppoSAX satellite was launched on April 30, 1996, in a low-earth low-inclination orbit with a height of about 600 km and an inclination angle of 4 deg. The near to equatorial orbit ensured the least disturbance by high-energy particle backgrounds from Cosmic Rays by taking full advantage of the screening effect of the Earth's magnetic field and avoiding most of the extreme particle flux in the polar regions and the South Atlantic Anomaly (SAA) which minimized the necessity to switch off the instruments during passages of such high flux portions of the orbit (Boella et al. 1997). Regular operations started in June and continued until April 30, 2002, for a total of 2156 d or 31 thousand satellite orbits. Apart from intermittent short periods due to operational incidents, the science instruments were turned off for longer periods during May-August 1997 to install the one-gyro mode, and during October 2001 to install the gyro-less mode. Furthermore, WFC unit 1 was turned off in May 1998 to let it recover from presumable frost bite. The total net time that the high voltage (HV) of the proportional counters was at a normal operational level was 1285 days for unit 1 and 1353 days for unit 2. These numbers are impacted by the fact that not always sufficiently accurate star tracker is available to infer the pointing information of the WFC within a few arcminutes. This reduces the useful observation time by 35%. Finally, the nearby earth often obscures (parts of) the field of view. Only 44% of the time the earth is completely outside the field of view of a WFC camera.

Both WFC cameras continuously observed the X-ray sky, except for times when the earth blocked the field of view or when the satellite passed the SAA. In the latter case, the cameras were put in standby mode by lowering the high voltage. Including times when the earth occulted (part of) the field of view, the sum of the exposure times of both cameras when the pointing was stable and known is 5.33 years or approximately 168 million seconds. In Fig. 1, a Galactic map of the coverage is given. The WFC did not provide a uniform coverage of the sky. In particular, fields around the Galactic center, the Galactic plane, the Crab nebula (opposite the Galactic center), Cygnus and LMC are more exposed. The Galactic center and Crab nebula fields were the primary targets for the WFC among the BeppoSAX instruments. The maximum coverage was obtained on the ecliptic poles (due to absence of earth occultations there) and is approximately 13 million seconds.

The WFC sensitivity ranged from $10^{-9} \text{ erg s}^{-1} \text{ cm}^{-2}$ (2-10 keV) for a time scale of 10 s, to a few times $10^{-11} \text{ erg s}^{-1} \text{ cm}^{-2}$ for a time scale of 10^5 s. This implies that it was not sensitive to detect flashes like were discovered by Gotthelf et al. (1996) in Einstein data or Sun et al. (1998) in ROSAT data. On the other hand, the WFC sensitivity is comparable to that of EP WXT for events shorter than about 50-100 s, while it does not reach the EP-WXT sensitivity for longer durations (see Sect. 7).

The GRBM was particularly used to detect GRBs. When a threshold was exceeded, the instruments triggered into high-resolution data collecting mode. The GRBM catalog of GRBs includes 1082 GRBs, one third of which was missed by the on-board trigger logic for various reasons and identified on ground using more sensitive algorithms (Frontera et al. 2009). Apart from GRB data, the instrument provided rate measurements at 1 s resolution and two bands: nominally 40-700 and >100 keV. For most of the FXTs reported here, these rate measurements are available. Of the 100 putative GRBs detected by the WFC, 79 were detected by the GRBM.

The Large Area Detectors (LADs) of the BATSE instrument were slightly more sensitive than the GRBM, particularly towards lower energies (the bandpass went down to 20 keV). They operated simultaneously with BeppoSAX for 3.8 yr, ending with the termination of the Compton Gamma Ray Observatory on 4 June 2000. Many of the events dealt with here did not activate BATSE's onboard trigger system which indicates that the 50-300 keV peak fluxes were below $0.2 \text{ phot s}^{-1} \text{ cm}^{-2}$ (1024 ms time scale). Like GRBM, BATSE was only sensitive to burst-like features with strong variability below 1 min time scales. Of the 65 GRBs detected by WFC before the end of CGRO, 27 GRBs were detected by BATSE. The remaining were probably mostly occulted by Earth as seen from CGRO in its low-earth orbit.

4. Search method and selection criteria

We searched for FXTs in the WFC database employing two different methods, each tailored to a specific time scale. They are as follows.

1. All time profiles of detector event rates, for both cameras and for whole detectors as well as quarters of detectors, were analyzed automatically as well as by eye at a resolution of 1 s in search of burst-like (sub-minute) events. When a candidate event was found, its reality was checked by generating a sky image for the duration of the event and searching for an accompanying point source. False events are usually due to solar activity (in extremely bright X-rays or particle winds) outside the field of view.
2. Sky images were generated in the complete bandpass for data stretches of 60 s, 300 s and 1 BeppoSAX orbit (1.5 hr) duration, sampling the data at intervals half the exposure time. These images were searched for sources that are otherwise quiescent in WFC data. The imaging algorithm was through cross correlation of the detector data with the mask pattern combined with Iterative Removal Of Sources (IROS; Hammersley 1986; Jager et al. 1997). For this, the detector spatial data were rebinned to $1 \times 1 \text{ mm}^2$ bins. Since the mask consists of 255×257 $1 \times 1 \text{ mm}^2$ bins, the cross correlation results in images of 510×512 pixels. The searches were done
 - a. on catalog positions of, for instance, flare stars within 100 pc in the lists of Kowalski (2024) and of stars that have shown flares in MAXI observations (29 stars). Detections were verified if they had a signal-to-noise ratio above a 3-sigma threshold;

¹ BATSE data is available at URL gamma-ray.nsstc.nasa.gov/batse/grb/

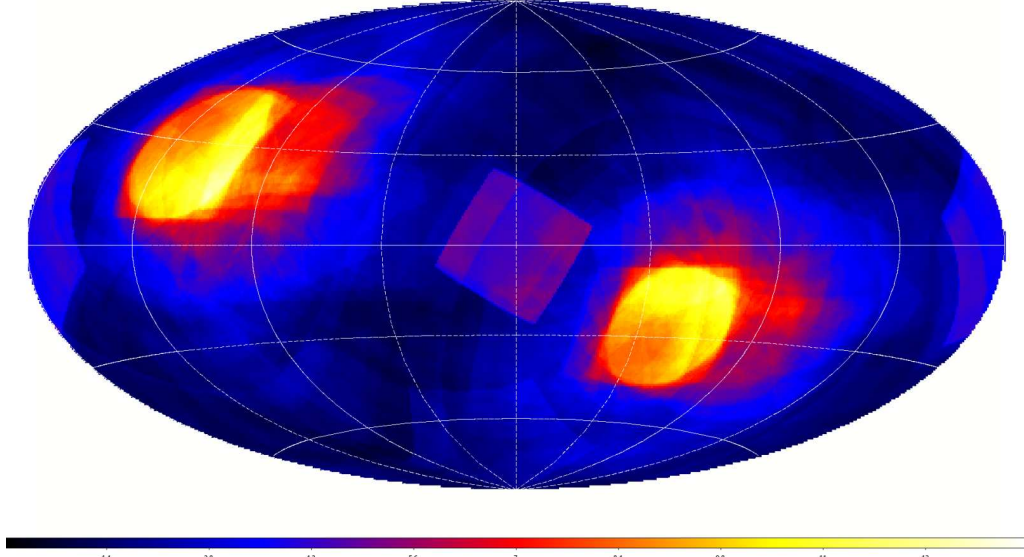


Fig. 1. Aitoff projection Galactic map of WFC exposure in units of Msec

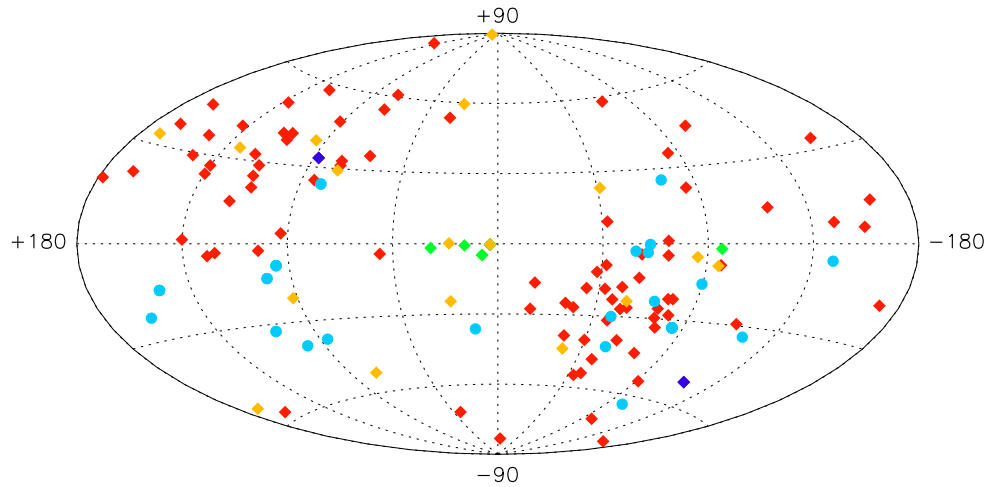


Fig. 2. Aitoff projection Galactic map of 149 FXTs. Red diamonds refer to GRBs, light blue to stellar flares, orange to unconfirmed GRBs ('GRB?' in Table 1), green-crossed o flares from X-ray binaries and dark blue to unconfirmed stellar flares

b. through blind searches in the whole field of view. The significance is used for selecting candidates. It refers to the flux divided by the expected Poisson noise in that flux and in most practical circumstances equals the signal-to-noise ratio. The significance threshold for verification was 5 sigma to allow less than 1 false detection in 510x512 sky pixels.

Verification was done by visually checking the reconstructed sky image for errors in the reconstruction (e.g., high noise levels for parts of the image) and, subsequently, generating light curves for the detected positions at time resolutions of 1, 10, 60, 300,

900 and 1800 s. If the light curves showed a clear temporary enhancement of the flux above the zero level over multiple time bins, the transient was validated.

There is one complication in the significance thresholds in the sky images. The calibration of the detector spatial response is not complete. On local scales, there are deviations from a flat response. This is typical for multi-wire proportional counters. It yields an overall systematic localization error of 0.7 arcmin (99% confidence). This imperfection makes it impossible to predict the image position of any point source any better than that, even if the celestial position is known at sub-arcsec accuracy as for most catalog sources. Thus, when searching for detections,

the point-spread function is fitted to any high signal-to-noise pixel with X and Y left free within boundaries of ± 3 pixels in our case. Obviously, this will bias the fitted flux to positive and negative stochastic noise fluctuations. Therefore, one has to increase the significance thresholds by a factor of $\sqrt{3}$, so up to 5.2 for catalog sources (point 2a above) and 8.2 for blind searches (2b).

Method 1 above results in the detection of many X-ray bursts (about 2500), mostly from cataloged X-ray binaries. Since these have all already been published in Galloway et al. (2020), we ignore them here. Also type-II bursts from the Rapid Burster and GRO J1744-28 are left out. We here concentrate on all other cases which concern GRBs, including X-ray flashes (XRFs), stellar flares and possibly AGN flares. This makes for a sample which can be compared with the early catalogs discussed in Sect. 1.

5. Catalog

Our search resulted in 149 FXT detections. Table 1 presents their basic parameters. The column description is as follows.

1. 'ID' - Identification, following the GRB convention of date at which the transient event occurred supplemented, for multiple events on a single day, with a rank letter from the alphabet;
2. 'Ref' - 'u' for unpublished event, 'a' for published by D'Alessio et al. (2006). Numbers refer to the papers cited in the footnote.
3. 'r' - an x denotes a case in which the community was alerted in near realtime (i.e., within hours) with the position of the event (55 cases). A + sign denotes a case where additionally the NFI observed the event within hours (38 cases²).
4. 'OP/WFC' - BeppoSAX observation identification ('Observation Period' or OP) and WFC unit that detected the event (1 or 2);
5. MJD(UTC) of the start of the event;
6. First of three columns that indicate timing behavior of the event. Column 5 indicates the duration of the event as estimated by eye in units of seconds except when indicated as h(ours), as is the estimated error which is indicated in the last digits between parentheses;
7. The rise time in minutes to the start of the final tail, in units of seconds; ;
8. Fitted e-folding decay time of the tail of the last peak of the event in units of minutes, with the 1-sigma uncertainty;
9. R.A. (eq. 2000.0) of the event, as determined from the centroid of the fitted point spread function and the attitude data of BeppoSAX. The position has been determined from the full-bandpass image with the optimum signal-to-noise ratio;
10. Dec. (eq. 2000.0);
11. The positional uncertainty of the event, expressed as the radius of the 99%-confidence circular error region, in units of arcmin. This is according to the calibration as discussed in Heise et al. (1998b). The 'P' label indicates additional systematic uncertainties due to an unfavorable star tracker configuration;
12. The angular separation between the event position (columns 8 & 9) and the identified counterpart (last column) in arcmin. If there is no identified counterpart, as is the case in a number of GRBs without optical follow-up, this column is kept empty;
13. CGRO-BATSE counterpart id., or offline identification ('untrig.'). Note that BATSE ceased operations on June 4, 2000;
14. Peak fluxes: WFC 2-30 keV peak flux in $\text{ct s}^{-1} \text{cm}^{-2}$ / GRBM 40-700 keV peak count rate in ct s^{-1} per detector corrected by division with the cosine of the off-axis angle. Note that 1) the WFC flux for the Crab source is 2.1 $\text{cts s}^{-1} \text{cm}^{-2}$, which for a Crab-like spectrum translates to 2.0 and $3.3 \times 10^{-8} \text{ erg s}^{-1} \text{cm}^{-2}$ for 2-10 and 2-30 keV, respectively; 2) in case the GRBM peak flux is left blank, it was not possible to reliably infer a value because the transients lasts ~ 1 h which makes it impossible to distinguish it from changes in the background that have a similar time scale; 3) in case the GRBM peak flux is marked by 'n.a.', GRBM data is not available; 4) in case the WFC peak flux is marked with an asterisk, it is unreliable; 5) this is a WFC-based table, implying that in a number of cases the GRBM did not detect the event. The GRBM peak rate is not corrected for dead time, which introduces an error of 0.3% at maximum;
15. The spectral softness ratio between the WFC (2-30 keV) and GRBM (40-700 keV) peak fluxes, multiplied by a factor of 1000. Note that the peak fluxes in the two instruments are measured at the same time resolution as employed in Fig. 4 but not necessarily at the same time;
16. Type of event, based on the optical/radio counterpart (next column) or when there is a clear simultaneous gamma-ray signal. When there is no clear counterpart and no clear gamma-ray signal in either GRBM or BATSE, the type is labeled with a questionmark.
17. Identification of the event with the most likely counterpart of persistent emission. This column may also have facts of interest. One of these facts is whether D'Alessio et al. (2006) finds whether a GRB is X-ray rich ('XRR') or an X-ray flash without clear gamma-ray signal ('XRF'). Note that we have a different criterion for XRF (see Sect. 7).

A synopsis of Table 1 is the following. 149 transient events are listed of which 64 have not been published before. 100 events are from GRBs (of which 23 unpublished; c.f. Vetere et al. 2007). 70 are without GRBM counterpart (21 GRBs and 49 stellar flares). 11 events are from supergiant fast X-ray transients (SFXTs) or other high-mass X-ray binaries (HMXBs) and 38 from flaring stars. Nine sources (2 SFXTs, 7 stars) are repeating between 1 and 6 times. The total number of unique sources in the table is 127, out of which 22 are stars (including 5 RS CVns, 3 BY Dra variables, 3 T Tau stars and 2 G-type stars), 4 SFXTs, 1 HMXBs and 100 GRBs/XRFs. 18 events have tentatively been identified as GRBs, but without the detection of a gamma-ray signal by the GRBM, BATSE or any other instrument.

Figure 2 shows a Galactic map of all 149 transients. The distribution is not isotropic as it reflects the non-isotropic coverage of WFC observations, see Figure 1.

Figure 3 shows the light curves of 49 transient events that can be attributed to stars and X-ray binaries. All data are shown of subsequent observations that continuously pointed at the source. Usually this concerns one OP, but occasionally this concerns up to 5 OPs. For all data we applied the standard allowed star tracker configurations. Furthermore, we included in this data set those data where the source radiation traverses at least 150 km above the earth horizon. During some of these data, the earth may obscure other parts of the field of view. For the light curve of event 010315 (GT Mus), a further constraint was applied where the earth was required to be completely out of the field of view, as in this particular case the standard star tracker configuration was unacceptable when the earth was in the field view (the flux of GT Mus would drop to zero during these times).

² See URL www.mpe.mpg.de/~jcg/grbgen.html and references therein

Figure 4 shows the light curves of the 100 GRBs, focusing on times closer to the (shorter) events. Also shown are the 5-30/2-5 keV spectral hardness ratio and the GRBM photon count rates. The latter data are raw data without background subtraction, in contrast to the WFC light curves. The same selection of good time intervals was applied as for Fig. 3 (allowed star tracker configurations and a source that is at least 150 km above the earth horizon).

We note that very bright events (i.e., 10 Crabs or brighter) were excluded on 971010 (MJD 50731.505104, OP2622, WFC unit 2), 000305 (51608.175961, 8616, 1) and 000411 (51645.119576, 8902, 2) because they exhibit a suspect top-hat light curve with a duration of 10-16 s.

6. Analysis

We have extracted overall WFC spectra of all 149 events, integrating over the duration of each event. These spectra were fitted with 3 models: a power law, a black body spectrum and thermal bremsstrahlung. All spectra were absorbed with XSPEC model ‘phabs’, with cross sections according to Balucinska-Church & McCammon (1992) and abundances according to Anders & Grevesse (1989). A narrow emission line

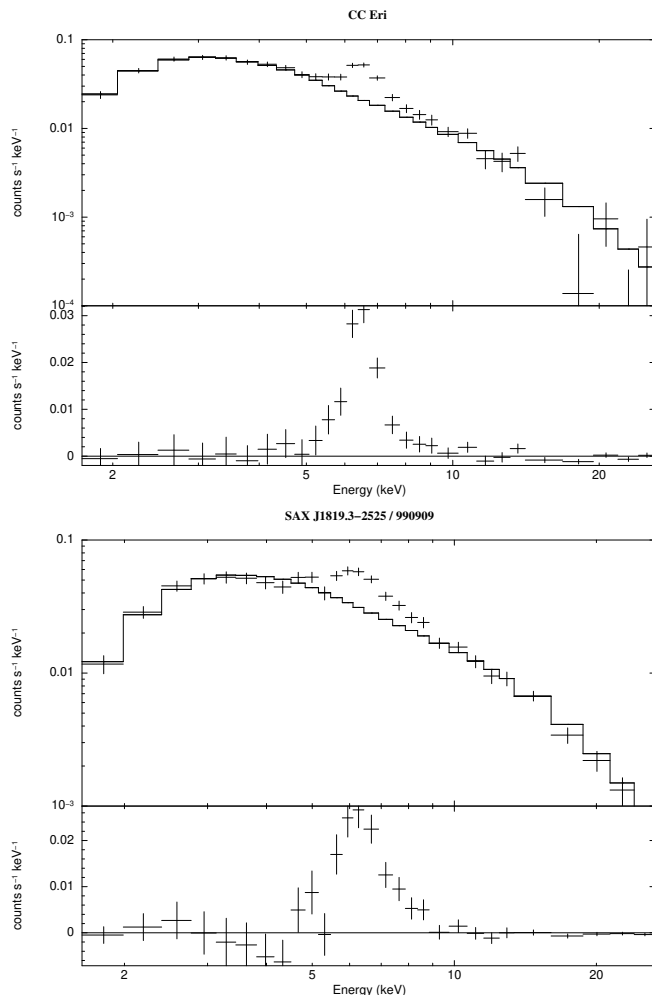


Fig. 5. Spectra showing strong Fe-K emission lines for CC Eri and SAX J1819.3-2525 on top of power-law continuum models. The equivalent widths of these two cases are 2.22 ± 0.15 and 1.62 ± 0.15 keV, respectively. The line widths have been fixed at 0 keV. The line of SAX J1819.3-2525 has been discussed in in’t Zand et al. (2001).

Table 3. Five most significant iron line detections in stellar flares

Event	Source	E(line) (keV)	EW (keV)	Signi- cance
970123	BY Dra	6.52 ± 0.13	1.63	5.0
970321	1RXS J214641.1...	6.56 ± 0.15	2.01	4.7
990909	SAX J1819.3-2525	6.38 ± 0.06	1.62	11.1
001207	CC Eri	6.61	2.22	14.8
010119	Algol	6.61	2.13	5.9

Table 4. Fitted values for N_{H} if left free. The uncertainties in the last digits are given between parentheses.

Event	Source	N_{H} (cm $^{-2}$)
960813	IGR J17544-2619 1	1.74(14)
970321	1RXS J214641.1-854303	2.35(11)
971018	AB Dor 1	2.66(27)
980218	AB Dor 2	2.27(39)
980311	SAX J1818.6-1703	3.08(97)
981102	AB Dor 3	2.75(38)
990220a	SAXJ 1819.3-2525 3	6.28(3.02)
990220b	IGR J17544-2619 2	1.36(20)
990311	IGR J17544-2619 6	2.53(48)
990911	IGR J17544-2619 3	1.49(15)
990909	SAX J1819.3-2525 2	1.77(6)
991005	AB Dor 4	2.12(24)
000409	AB Dor 5	2.10(21)
000920	IGR J17544-2619 4	4.19(70)
001008	IGR J17544-2619 5	2.00(31)
010301	AB Dor 6	2.39(14)
010304b	IGR J08408-4503	2.33(68)
010315	GT Mus	1.76(8)
010324b	AX J1845.0-0433	2.49(42)
010327	AB Dor 7	2.57(34)

was included at the energy of the Fe K line. In general, the fits with the power law are best. 11% of the black body fits show lower χ^2_{r} and 39% of the bremsstrahlung fits. However, in all these cases the quality of the fits is similar for the power law fits. Therefore, for the remainder we only consider the power law fits. Interstellar absorption and a narrow line were set to zero except for a few cases where they were necessary to obtain a good fit. Table 2 presents the results of the spectral analysis with a power law, including a presentation of the 2-30 keV fluence and 2-30 keV isotropic energy output for all cases for which a distance is known. Three groups are discernable in distance and, therefore, energy output: nearby stellar flares (10^{34} - 10^{38} erg), flares from X-ray binaries at a few kpc ($\sim 10^{40}$ erg) and GRBs ($\sim 10^{51}$ erg). See Tables 3 and 4 for cases where an emission line was included at the Fe K location and N_{H} was left free, respectively.

For 5 stellar flares the inclusion of the emission line at ≈ 6.5 keV was necessary for a good fit. The 5 cases are in decreasing order of significance: 001207 (flare from CC Eri), 990909 (first flare from SAX J1819.3-2525), 010119 (third flare from Algol), 970321 (flare from 1RXS J214641.1-854303) and 970123 (first flare from BY Dra), see Table 3. The two most significant Fe-K lines are shown in Fig. 5. Note that none of the GRB average spectra showed a significant Fe-K emission line. However, some bursts have transient narrow spectral features in WFC data: GRB990705 (Amati et al. 2000), GRB990712 (Frontera et al. 2001) and GRB011211 (Frontera et al. 2004).

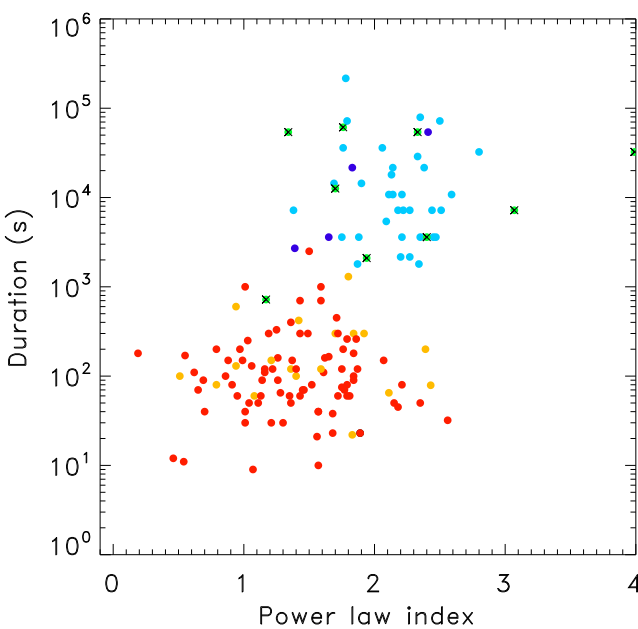


Fig. 6. Diagram of duration versus power law photon index for all events. Red dots refer to GRBs, light blue to stellar flares, orange to unconfirmed GRBs ('GRB?' in Table 1), green-crossed to flares from X-ray binaries and dark blue to unconfirmed stellar flares.

Figure 6 shows the diagram of duration versus power-law photon index. The duration is copied from column 5 of Table 1. The 5 different types of sources are indicated with different colors. GRBs and stellar flares are clearly distinct in this diagram. GRBs are short and hard (low photon index), while stellar flares are the opposite. The uncertain classes are mostly associated with GRBs without gamma-ray signals ('GRB?' in Table 1, orange symbols in Fig. 6).

Since the uncertain GRB cases are all without a GRBM signal or data, they did not trigger realtime alerts to the community and follow-up observations with, among instruments elsewhere, the NFI. Thus, the WFC data are the only data on these events. There is one exception, GRB991217, which triggered a prompt reaction because of the strong WFC signal and a noise peak in the GRBM data. No NFI observation took place but optical follow up was engaged with 1 m class telescopes. Unfortunately, no afterglow was detected brighter than $R \approx 22$ within 0.5-2.5 d (Mohan et al. 1999).

Considering that the brightest X-ray stellar flares have a luminosity of 10^{32} erg s $^{-1}$, this implies that stellar flares can be detected by the WFC (taking a sensitivity of 2×10^{-10} erg s $^{-1}$ cm $^{-2}$ for duration of about 1000 s) to a maximum distance of 64 parsecs, which ensures the completeness of star catalogue (Gaia Collaboration et al. 2023). The association of the uncertain GRBs to X-ray-dominated GRBs, i.e. XRFs, is supported by the fact that these events share the same duration-spectral index region populated by GRBs (Fig. 6).

There are a few unidentified longer cases that are on the border between GRBs and stellar flares. They are the two events from GR Dra and the two events from SAX J0346.6-3906 (dark blue symbols in Fig. 6). These are further discussed in Sect. 6.1.

6.1. Interesting individual cases

6.1.1. GR Dra

Williams et al. (1995, 1997) reported the detection in November 1992 with CGRO-Comptel of the MeV transient GRO J1753+57. The source was detected in two consecutive 14-d 'viewing periods' (VPs) with a 1-3 MeV peak flux in one VP of 10^{-6} ph s $^{-1}$ cm $^{-2}$. This flux equals half the flux of the Crab source in the same bandpass. The spectrum is consistent with that of an AGN. Within the 4 deg error radius of the source (4-sigma confidence), 14 candidate counterparts were identified which are not galaxy clusters. 3 of them are stars, 7 are AGN and 4 are of unknown type. By virtue of the similarity in gamma-ray behavior to 2 other transients, the source was suspected to be of AGN origin. Carramiñana et al. (1997) searched for optical counterparts among 9 radio sources and 10 AGN in the error region but was unsuccessful in finding a clear variable counterpart.

We find two transient events in our catalog whose positions are consistent with that of one of the candidates identified by Williams as counterpart: 1ES 1727+590 = GR Dra. This object is, at 3.6 deg from the centroid position of GRO 1753+57, the third closest of nine. Therefore, we conclude that we have detected the second and third outburst of the MeV transient GRO 1753+57 but now at 2-30 keV instead of 1-10 MeV and that it is a Galactic star rather than of extragalactic origin. The WFC-detected flares are much shorter than 4 weeks as observed by CGRO-Comptel. This suggests that the transient event seen by CGRO may comprise of multiple events in 2 VPs.

The peak flux that we observe, about 0.08 phot s $^{-1}$ cm $^{-2}$, is about 40 mCrab. Thus, the 0.5 Crab flux measured by CGRO suggests a hard MeV tail. The X-ray spectrum is rather soft, with a photon index of 2 or a bremsstrahlung temperature of 4.6 keV.

What type of star is GR Dra? It is a bright ($V=8.26$) G0 star at a distance of 139 pc. Schachter et al. (1996) detects optical variability from this star. GR Dra exhibits persistent X-ray emission at a level of 1.4 mCrab (0.1-2.4 keV; Voges et al. 1999).

If GR Dra is the same as GRO 1753+57, how can a G0 star give rise to MeV transient emission? We suggest that GR Dra may house a compact object. Sensitive follow-up observations should be interesting.

6.1.2. SAX J0346.6-3906 = UCAC4 255-003783

We see two transient events lasting less than 1 hr and peaking at about 100 mCrab and with a moderately hard spectrum (photon index 1.8). There are no known X-ray sources at its location. There is one optical counterpart: UCAC4 255-003783, a cool star in the Epsilon Cha star association. Since SAX J0346.6-3906 is a repeating source, it cannot be a (long) GRB. The event may be a faint X-ray burst due to a distant X-ray binary. For a peak luminosity equal to the Eddington limit of a H-rich accreting neutron star, the distance would be ~ 30 kpc which would place it at a somewhat unlikely location outside the Galactic Bulge.

6.1.3. 1RXS J214641.1-854303 = NLTT 51688

This object has been identified with a $V=13.4$ M3.5 dwarf star NLTT 51688 (Riaz et al. 2006) at a distance of 16 pc (Gaia Collaboration et al. 2023), which has never been seen to flare before but whose spectral type is fully consistent with flaring activity. We detect a significant Fe-K line from this source,

which suggests that substantial obscuration of the flare source occurs.

6.1.4. 2RE J051724-352221 = CD-35 2213

This object has been identified with a $V=11.7$ M4Ve dwarf star (Scholz et al. 2005) at a distance of 12 pc (Gaia Collaboration et al. 2023), which has never been seen to flare before but whose spectral type is fully consistent with flaring activity.

6.1.5. Others

971019. This is the brightest and the softest GRB event. A combined WFC/BATSE spectral fit over the whole event shows a peak energy in the νF_ν spectrum of 19 ± 1 keV compared to an average peak energy of about 200 keV for classical GRBs (Kippen et al. 2003). This is the prototypical X-ray flash (XRF) case of our sample.

980306 is classified as XRF on the basis of BATSE data instead of GRBM data (Kippen et al. 2003). It was followed up with the BeppoSAX NFI on August 1-2, 1999, 17 months after the event. This observation is not yet discussed in the literature. No source was detected with MECS within the WFC error box above $1.7 \times 10^{-3} \text{ c s}^{-1}$ (3.5-sigma upper limit) corresponding to a flux of $\sim 10^{13} \text{ erg s}^{-1} \text{ cm}^{-2}$.

980429. This is the first XRF that was followed up with a sensitive device within a matter of days (Heise et al. 1998a). The NFI observed the position between 32.45 and 53.4 hrs after the flash and detected one source at a position of $\text{R.A.}_{2000.0} = 130.1507$ deg, $\text{Decl.}_{2000.0} = +22.8584$ deg with an uncertainty of 1.0. This is 1:1 from the WFC centroid, so fully consistent. The source is weak, with a MECS photon count rate of $(2.11 \pm 0.39) \times 10^{-3} \text{ s}^{-1}$ over 37364 s net exposure time, and no variability nor spectrum could be detected. The photon rate implies a 2-10 keV flux of a few times $10^{-13} \text{ erg s}^{-1} \text{ cm}^{-2}$. Since there is no clear decay during the NFI observation, the source cannot unambiguously be identified as the afterglow. Optical follow up after 2.8 d failed to find a counterpart, with limiting magnitudes of B~22 and R~21 (Djorgovski et al. 1998). This source was also followed up in 2007 and not detected above an upper limit of $4.5 \times 10^{-14} \text{ erg s}^{-1} \text{ cm}^{-2}$ (presumably in 0.5-10 keV; Romano et al. 2008).

991106. This event cannot be completely ruled out as a type-I X-ray burst (Cornelisse et al. 2002). The Galactic latitude of this event is -2.6 deg. This event was followed up with the NFI between 7.9 and 27.0 hr after the event. The MECS exposure time is 31.7 ksec, and the LECS exposure 11.8 ksec. The MECS data show a detection of a point source in the WFC error box. The flux is $1.8 \times 10^{-3} \text{ c s}^{-1}$ in the MECS, which for a Crab spectrum is roughly $10^{-13} \text{ erg s}^{-1} \text{ cm}^{-2}$ which is very low for an X-ray burster with such a short burst.

7. Discussion

The faintest FXT that we find has a peak WFC flux of $0.02 \text{ c s}^{-1} \text{ cm}^{-2}$ (and a duration of 20 h) which, for a Crab-like spectrum, translates to $2 \times 10^{-10} \text{ erg s}^{-1} \text{ cm}^{-2}$ (2-30 keV). For a 10^3 s exposure, the formal 5-sigma sensitivity is the same value (2-30 keV) for fields away from the Galactic center and for the on-axis position. For other positions in the field

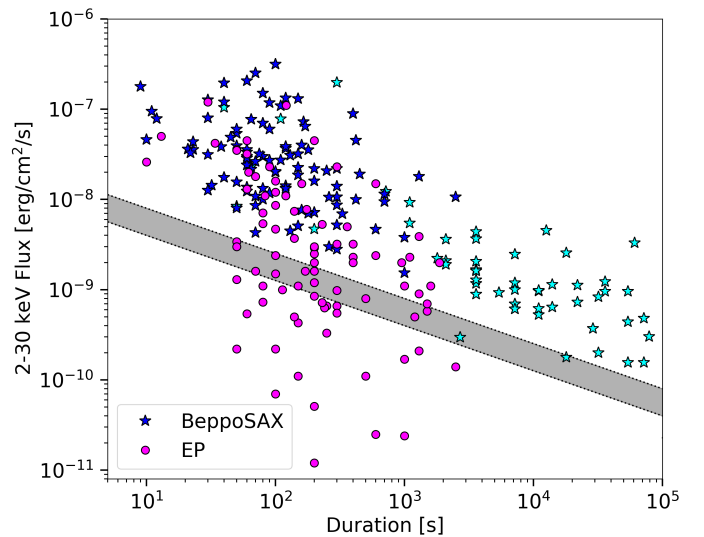


Fig. 7. Flux comparison of Einstein Probe and BeppoSAX events. 149 BeppoSAX-WFC GRBs and stars from the present catalog are represented in blue and cyan asterisk symbols, respectively. 84 EP-WXT transients (without stars and Galactic sources, from Wu et al. 2025; Aryan et al. 2025) are in magenta-filled circles. The WFC sensitivity is drawn as a grey band since it depends on the particular X-ray source configuration in any observed sky image.

of view, the sensitivity reduces approximately pyramidalically towards the edge and the average over the field of view is about $4 \times 10^{-10} \text{ erg s}^{-1} \text{ cm}^{-2}$.

Our coverage is 5.33 yr exposure for 2 WFC cameras times the 0.47 sr field of view of one WFC camera. This equals 2.50 yr sr and implies a yearly all-sky rate of $755 \pm 62 \text{ yr}^{-1}$. This is of the same order of magnitude as what was found with the detections by Ariel V and HEAO in the 1970s based on fewer events (Ambruster & Wood 1986; Pye & McHardy 1983).

An interesting comparison to make is with the recent results from the WXT on EP. From General Coordinate Network (GCN) circulars of the first year of EP operations, Wu et al. (2025) collected 128 FXTs, including stellar flares and known sources, while Aryan et al. (2025) collected 72 FXTs, excluding stellar flares. For a field of view of 1.1 sr and assuming an observation efficiency of 90%, this yields a total all-sky rate of GRBs and stellar flares of roughly $1600 \pm 140 \text{ yr}^{-1}$. This is a factor of 2 higher than for the WFC. This can roughly be explained by a difference in sensitivity. The WXT sensitivity is $0.26 \times 10^{-10} \text{ erg s}^{-1} \text{ cm}^{-2}$ (0.5-4 keV) for an exposure time of 10^3 s. EP-WXT has a better sensitivity than BeppoSAX-WFC for events lasting longer than about 100 s, because the WXT is photon limited, it being an direct focusing camera, while the WFC is background limited. In Fig. 7, we plot the average flux in the 2-30 keV range versus duration for events detected by either WFC or WXT. Here, the EP-WXT flux has been extrapolated from 0.5-4 keV to 2-30 keV using the published WXT spectra and, therefore, does not take into account any possible spectral breaks between 4 and 30 keV. When we consider only the 50 EP events above the BeppoSAX-WFC sensitivity (taking the center line of grey region as dividing line), the fraction of EP events that would be detectable by the WFC is 0.61. If we correct the value of 1600 above for this fraction, the all-sky rates of transients are comparable: the EP rate reduces to 960 ± 221 , a factor of 1.27 ± 0.24 higher than the WFC rate. Systematic effects, for

instance due to the different bandpasses of the WFC and WXT, will add uncertainty to this number.

Another interesting comparison to make is with MAXI. According to the MAXI alert messages disseminated through email, MAXI has detected 150 stellar flares in 15 years from 29 unique stars which translates to a yearly all-sky rate of approximately 15 yr⁻¹ above a sensitivity threshold of about 6×10^{-10} erg s⁻¹cm⁻² (2-30 keV Matsuoka et al. 2009). This is substantially lower than WFC, WXT and other missions. Parts of this can be explained by the worse sensitivity and an incomplete count on our part from the literature. MAXI has a large sky coverage for events that last longer than one MAXI orbit and should be quite efficient in detecting these.

The census of late-type main sequence stars is complete for distances of up to about 200 pc from GAIA measurements, for a limiting G magnitude of 21 (Gaia Collaboration et al. 2023). Pye et al. (2015) determine an X-ray peak flux range for stellar flares of 10^{27} - 10^{32} erg s⁻¹. The WFC sensitivity limit of 2×10^{-10} erg s⁻¹cm⁻² implies that even for the smallest distance of 1 pc, not the whole range of peak fluxes of stellar flares can be detected. Thus, the reach of WFC detections is smaller than that of optical detections of late-type stars. Therefore, any WFC detection of a stellar flare should be identifiable through an optical counterpart and this is indeed the case.

We identified 33 stellar flares by cross checking positions with catalogs of stars (e.g., Kowalski 2024). The location of an additional event is coincident with ROSAT source 1RXS J214641.1-854303 and M3.5 star NLTT 51688, a probable flare star. Four further flares were detected from sky regions that are not known to host a known flare star. These have been tentatively identified with other counterparts, one which exhibited gamma-ray flares in the 1990s (GR Dra) and one with a cool star (UCAC4 255-003783). Therefore, 87% of the long-duration/soft events could be unambiguously identified through obvious counterparts.

42% of the FXTs reported here have not been reported previously. This applies to 37 out of 38 stellar flares, 3 SFXTs and 23 out of 100 GRBs. This is unfortunate for this revolutionizing phase of GRB research when the distance scale of GRBs was first established. The reason is that the missed-out GRBs are mostly gamma-ray poor. This prevented quick-look recognition of GRBs in the GRBM and quick follow-up in WFC data for localization, specially in the early phase of the mission lifetime. However, some were recognized in real time and triggered broad band follow-up observations. It was then realized that they were at similar distances as GRBs and exhibited broad-band afterglows not unlike GRB, motivating the association of XRF to a class of GRBs (e.g., Piro et al. 2005; Galli & Piro 2006; Amati et al. 2004). This association has been further consolidated following the lauch of HETE II (Lamb et al. 2004) and Swift (Gehrels et al. 2009), with XRF sample studies of the joint BeppoSAX-HETE-2 sample (D'Alessio et al. 2006; Sakamoto et al. 2005) and Swift (Sakamoto et al. 2008)

If we apply a peak flux softness ratio threshold of 16 or larger, above which we fail to detect a GRBM signal for most GRBs, for XRFs we find 37 such cases or 37% of all GRBs. This is roughly consistent with earlier findings, although those make a distinction between 3 classes rather than 2 and apply thresholds to different definitions of spectral hardness ratios: X-ray flashes ($H_s > 1$ with H_s =fluence(2-30 keV)/fluence(40-400 keV), X-ray rich GRBs ($0.32 < H_s < 1$) and classical GRBs ($H_s < 0.32$) (D'Alessio et al. (2006), see also Sakamoto et al. (2005)). Note that the hardest GRBs in our sample have a softness ratio of 0.8 (GRB990123 and GRB000210). These rates are slightly dif-

ferent compared to the sample detected by EP-WXT. For example, Zhang et al. (2025b) find that 22% of FXTs detected by EP-WXT have a gamma-ray counterpart, searching in GECAM and Fermi/GBM data. This difference likely arises from the better sensitivity of EP-WXT, which can detect transients as faint as few in 10^{-11} erg s⁻¹cm⁻². The difference in the rates could also be due, in part, to the different band passes of the GRBM, with respect to Fermi-GBM (8 keV – 40 MeV) and GECAM (10 keV – 6 MeV). Instead, the GRBM sensitivity is comparable to Fermi-GBM and GECAM (order of 10^{-8} erg s⁻¹cm⁻²).

The science goal of the WFC, when the instrument was proposed in the 1980s, was the multiplication of data on FXTs to better determine their origin. The WFC has detected about 2700 FXTs in the categories of thermonuclear flashes on accreting neutron stars (≈ 2500), GRBs (100), stellar flares (38), SFXT flares (11) and type-II X-ray bursts (uncounted). The first-time fast (within hours) and accurate (within arcmin) localization of GRBs solved the decades-long enigmatic mystery of their origin. The plentitude of thermonuclear flashes doubled the known population of such sources and surfaced a special type of thermonuclear flash ('superburst', Cornelisse et al. (2000) fueled by carbon (like type Ia SNe). The topping off with stellar flares has made the identification possible of 99% of all FXTs and explained their origin. The conclusion is that the WFC instrument has met its science goal.

Acknowledgements. We are indebted to retired SRON colleagues Gerrit Wiersma and Jaap Schuurmans for their invaluable assistance in the data reduction of WFC data, and to Wim Mels, Rieks Jager and Frank van Beek for leading the instrument development of the WFC. LP and GG acknowledge support from ASI (Italian Space Agency) through contract no. 2019-27-HH.0. This research has made use of the SIMBAD database, operated at CDS, Strasbourg, France, NASA's Astrophysics Data System Bibliographic Services and Jochen Greiner's compendium of GRBs available at URL www.mpe.mpg.de/~jcg/grbgen.html.

Author contributions. Data extraction: JZ and CG. Data analysis: JZ, LP and GG. Manuscript preparation: JZ. Manuscript review and improvement: all authors. It is noted that no AI tool has been employed in the data reduction analysis nor manuscript preparation.

References

- Amati, L., Cinti, M. N., Feroci, M., et al. 1997, in Society of Photo-Optical Instrumentation Engineers (SPIE) Conference Series, Vol. 3114, EUV, X-Ray, and Gamma-Ray Instrumentation for Astronomy VIII, ed. O. H. Siegmund & M. A. Gummin, 176–185
- Amati, L., Frontera, F., in't Zand, J. J. M., et al. 2004, A&A, 426, 415
- Amati, L., Frontera, F., Vietri, M., et al. 2000, Science, 290, 953
- Ambruster, C. W. & Wood, K. S. 1986, ApJ, 311, 258
- Anders, E. & Grevesse, N. 1989, Geochim. Cosmochim. Acta, 53, 197
- Antonelli, L. A., Fiore, F., Amati, L., et al. 1999a, A&AS, 138, 435
- Antonelli, L. A., Nicastro, L., Daniele, M. R., et al. 1999b, GRB Coordinates Network, 359, 1
- Antonelli, L. A., Piro, L., Vietri, M., et al. 2000, ApJ, 545, L39
- Arefiev, V. A., Priedhorsky, W. C., & Borozdin, K. N. 2003, ApJ, 586, 1238
- Aryan, A., Chen, T.-W., Yang, S., et al. 2025, ApJS, 281, 20
- Balucinska-Church, M. & McCammon, D. 1992, ApJ, 400, 699
- Boella, G., Butler, R. C., Perola, G. C., et al. 1997, A&AS, 122, 299
- Brinkman, A. C., Dam, J., Mels, W. A., Skinner, G. K., & Willmore, W. P. 1985, in Non-thermal and Very High Temperature Phenomena in X-ray Astronomy, ed. G. C. Perola & M. Salvati, 263
- Carramiñana, A., Chavushyan, V., & Guichard, J. 1997, in American Institute of Physics Conference Series, Vol. 410, Proceedings of the Fourth Compton Symposium, ed. C. D. Dermer, M. S. Strickman, & J. D. Kurfess (AIP), 1462–1466
- Celidonio, G., Coletta, A., Feroci, M., et al. 1998, IAU Circ., 6851, 1
- Connors, A., Serlemitos, P. J., & Swank, J. H. 1986, ApJ, 303, 769
- Cornelisse, R., Heise, J., Kuulkers, E., Verbunt, F., & in 't Zand, J. J. M. 2000, A&A, 357, L21
- Cornelisse, R., Verbunt, F., in 't Zand, J. J. M., et al. 2002, A&A, 392, 885

Corsi, A., Piro, L., Kuulkers, E., et al. 2005, *A&A*, 438, 829

Costa, E., Feroci, M., Piro, L., et al. 1997a, *IAU Circ.*, 6533, 1

Costa, E., Frontera, F., dal Fiume, D., et al. 1998, *Advances in Space Research*, 22, 1129

Costa, E., Frontera, F., Heise, J., et al. 1997b, *Nature*, 387, 783

Dal Fiume, D., Amati, L., Antonelli, L. A., et al. 2000, *A&A*, 355, 454

D'Alessio, V., Piro, L., & Rossi, E. M. 2006, *A&A*, 460, 653

Djorgovski, S. G., Kulkarni, S. R., Kollmeier, J., Frail, D. A., & Caltech GRB Collaboration. 1998, *GRB Coordinates Network*, 66, 1

Fenimore, E. E. & Cannon, T. M. 1978, *Appl. Opt.*, 17, 337

Feroci, M., Antonelli, L. A., Soffitta, P., et al. 2001, *A&A*, 378, 441

Feroci, M., Frontera, F., Costa, E., et al. 1997, in *Society of Photo-Optical Instrumentation Engineers (SPIE) Conference Series*, Vol. 3114, EUV, X-Ray, and Gamma-Ray Instrumentation for Astronomy VIII, ed. O. H. Siegmund & M. A. Gummin, 186–197

Fishman, G. J., Meegan, C. A., Wilson, R. B., et al. 1994, *ApJS*, 92, 229

Fishman, G. J., Woods, P. M., Hossfield, C., & Anderson, L. 2002, *GRB Coordinates Network*, 1394, 1

Frontera, F., Amati, L., in 't Zand, J. J. M., et al. 2004, *ApJ*, 616, 1078

Frontera, F., Amati, L., Vietri, M., et al. 2001, *ApJ*, 550, L47

Frontera, F., Antonelli, L. A., Amati, L., et al. 2000, *ApJ*, 540, 697

Frontera, F., Costa, E., dal Fiume, D., et al. 1997, *A&AS*, 122, 357

Frontera, F., Guidorzi, C., Montanari, E., et al. 2009, *ApJS*, 180, 192

Gaia Collaboration, Vallenari, A., Brown, A. G. A., et al. 2023, *A&A*, 674, A1

Galli, A. & Piro, L. 2006, *A&A*, 455, 413

Galloway, D. K., in 't Zand, J., Chenevez, J., et al. 2020, *ApJS*, 249, 32

Gehrels, N., Ramirez-Ruiz, E., & Fox, D. B. 2009, *ARA&A*, 47, 567

Gianfagna, G., Piro, L., Bruni, G., et al. 2025, *A&A*, 703, A92

Gotthelf, E. V., Hamilton, T. T., & Helfand, D. J. 1996, *ApJ*, 466, 779

Guidorzi, C., Frontera, F., Montanari, E., et al. 2003, *A&A*, 401, 491

Guidorzi, C., Montanari, E., Frontera, F., et al. 2001, *GRB Coordinates Network*, 1021, 1

Hammersley, A. P. 1986, PhD thesis, -

Heise, J., Brinkman, A. C., Schrijver, J., et al. 1975, *ApJ*, 202, L73

Heise, J., in 't Zand, J., Ricci, R., et al. 1998a, *IAU Circ.*, 6892, 1

Heise, J., in 't Zand, J. J. M., Muller, J. M., et al. 1998b, in *American Institute of Physics Conference Series*, Vol. 428, Gamma-Ray Bursts, 4th Hunstville Symposium, ed. C. A. Meegan, R. D. Preece, & T. M. Koshut (AIP), 397–403

Heise, J., Zand, J. I., Kippen, R. M., & Woods, P. M. 2001, in *Gamma-ray Bursts in the Afterglow Era*, ed. E. Costa, F. Frontera, & J. Hjorth, 16

in 't Zand, J., Heise, J., Smith, M., et al. 1998a, *IAU Circ.*, 6840, 2

in 't Zand, J., Muller, J. M., Piro, L., et al. 1998b, *IAU Circ.*, 6805, 1

in 't Zand, J. J. M., Heise, J., & Jager, R. 1994, *A&A*, 288, 665

in 't Zand, J. J. M., Kuiper, L., Amati, L., et al. 2000, *ApJ*, 545, 266

in 't Zand, J., Heise, J., Ubertini, P., Bazzano, A., & Markwardt, C. 2004a, in *ESA Special Publication*, Vol. 552, 5th INTEGRAL Workshop on the INTEGRAL Universe, ed. V. Schoenfelder, G. Lichten, & C. Winkler, 427

in 't Zand, J. J. M., Heise, J., Kippen, R. M., et al. 2004b, in *Astronomical Society of the Pacific Conference Series*, Vol. 312, Gamma-Ray Bursts in the Afterglow Era, ed. M. Feroci, F. Frontera, N. Masetti, & L. Piro, 18

in 't Zand, J. J. M., Kuiper, L., Amati, L., et al. 2001, *ApJ*, 559, 710

in 't Zand, J. J. M., Kuulkers, E., Bazzano, A., et al. 2000, *A&A*, 357, 520

Jager, R., Mels, W. A., Brinkman, A. C., et al. 1997, *A&AS*, 125, 557

Kippen, R. M., Woods, P. M., Heise, J., et al. 2003, in *American Institute of Physics Conference Series*, Vol. 662, Gamma-Ray Burst and Afterglow Astronomy 2001: A Workshop Celebrating the First Year of the HETE Mission, ed. G. R. Ricker & R. K. Vanderspek (AIP), 244–247

Kowalski, A. F. 2024, *Living Reviews in Solar Physics*, 21, 1

Kumar, P. & Zhang, B. 2015, *Phys. Rep.*, 561, 1

Kuulkers, E., Antonelli, L. A., Kuiper, L., et al. 2000, *ApJ*, 538, 638

Lamb, D. Q., Ricker, G. R., Atteia, J.-L., et al. 2004, *New A Rev.*, 48, 423

Lawson, W. A., Crause, L. A., Mamajek, E. E., & Feigelson, E. D. 2002, *MNRAS*, 329, L29

Li, D.-Y., Zhang, W.-D., Yang, J., et al. 2025, *arXiv e-prints*, arXiv:2509.25877

Liu, Y., Sun, H., Xu, D., et al. 2025, *Nature Astronomy*, 9, 564

Matsuoka, M., Kawasaki, K., Ueno, S., et al. 2009, *PASJ*, 61, 999

Mels, W. A., Lowes, P., Burmans, H. B., et al. 1988, *Nuclear Instruments and Methods in Physics Research A*, 273, 689

Mohan, V., Sagar, R., Pandey, A. K., et al. 1999, *GRB Coordinates Network*, 502, 1

Montanari, E., Amati, L., Frontera, F., et al. 2001, in *Gamma-ray Bursts in the Afterglow Era*, ed. E. Costa, F. Frontera, & J. Hjorth, 195

Muller, J. M., Kuulkers, E., Tarei, G., et al. 1999, *GRB Coordinates Network*, 474, 1

Nicastro, L., Amati, L., Antonelli, L. A., et al. 1998, *A&A*, 338, L17

Osten, R. A., Godet, O., Drake, S., et al. 2010, *ApJ*, 721, 785

Paciesas, W. S., Meegan, C. A., Pendleton, G. N., et al. 1999, *ApJS*, 122, 465

Pian, E., Amati, L., Antonelli, L. A., et al. 1999, *A&AS*, 138, 463

Piro, L. 1999, *GRB Coordinates Network*, 355, 1

Piro, L., De Pasquale, M., Soffitta, P., et al. 2005, *ApJ*, 623, 314

Piro, L., Frail, D. A., Gorosabel, J., et al. 2002, *ApJ*, 577, 680

Piro, L., Heise, J., Jager, R., et al. 1998, *A&A*, 329, 906

Proctor, R. J., Skinner, G. K., & Willmore, A. P. 1978, *MNRAS*, 185, 745

Pye, J. P. & McHardy, I. M. 1983, *MNRAS*, 205, 875

Pye, J. P., Rosen, S., Fyfe, D., & Schröder, A. C. 2015, *A&A*, 581, A28

Quiroga-Vásquez, J., Bauer, F. E., Jonker, P. G., et al. 2022, *A&A*, 663, A168

Rappaport, S., Buff, J., Clark, G., et al. 1976, *ApJ*, 206, L139

Riaz, B., Gizis, J. E., & Harvin, J. 2006, *AJ*, 132, 866

Ricci, R., D'Andretta, G., Costa, E., et al. 1998, *IAU Circ.*, 6910, 2

Romano, P., Guidorzi, C., Sidoli, L., et al. 2008, in *American Institute of Physics Conference Series*, Vol. 1000, Gamma-ray Bursts 2007, ed. M. Galassi, D. Palmer, & E. Fenimore (AIP), 146–149

Sakamoto, T., Hullinger, D., Sato, G., et al. 2008, *ApJ*, 679, 570

Sakamoto, T., Lamb, D. Q., Kawai, N., et al. 2005, *ApJ*, 629, 311

Schachter, J. F., Remillard, R., Saar, S. H., et al. 1996, *ApJ*, 463, 747

Scholz, R.-D., Meusinger, H., & Jahreiß, H. 2005, *A&A*, 442, 211

Seli, B., Vida, K., Oláh, K., et al. 2025, *A&A*, 694, A161

Skinner, G. K., Willmore, A. P., Eyles, C. J., Bertram, D., & Church, M. J. 1987, *Nature*, 330, 544

Sun, H., Li, W.-X., Liu, L.-D., et al. 2025, *Nature Astronomy*, 9, 1073

Sun, X., Li, H., Fenimore, E. E., & Wang, Q. D. 1998, in *American Institute of Physics Conference Series*, Vol. 428, Gamma-Ray Bursts, 4th Hunstville Symposium, ed. C. A. Meegan, R. D. Preece, & T. M. Koshut (AIP), 456–460

Tsubo, Y., Akasu, K., Nemoto, N., et al. 2024, in *Society of Photo-Optical Instrumentation Engineers (SPIE) Conference Series*, Vol. 13093, Space Telescopes and Instrumentation 2024: Ultraviolet to Gamma Ray, ed. J.-W. A. den Herder, S. Nikzad, & K. Nakazawa, 1309366

Tsubo, Y., & Sasaki, R. 2020, in *Multifrequency Behaviour of High Energy Cosmic Sources - XIII*, 3–8 June 2019, Palermo, 54

van den Oord, G. H. J. & Mewe, R. 1989, *A&A*, 213, 245

van Paradijs, J., Groot, P. J., Galama, T., et al. 1997, *Nature*, 386, 686

Vetere, L., Soffitta, P., Massaro, E., Giommi, P., & Costa, E. 2007, *A&A*, 473, 347

Voges, W., Aschenbach, B., Boller, T., et al. 1999, *A&A*, 349, 389

Williams, O. R., Bennett, K., Much, R., et al. 1997, in *American Institute of Physics Conference Series*, Vol. 410, Proceedings of the Fourth Compton Symposium, ed. C. D. Dermer, M. S. Strickman, & J. D. Kurfess (AIP), 1243–1247

Williams, O. R., Much, R., Bennett, K., et al. 1995, *A&A*, 297, L21

Willmore, A., Skinner, G., Eyles, C., & Ramsey, B. 1984, *Nuclear Instruments and Methods in Physics Research*, 221, 284

Wu, S., Pérez-García, I., Castro-Tirado, A. J., et al. 2025, *Galaxies*, 13, 62

Yuan, W., Dai, L., Feng, H., et al. 2025, *Science China Physics, Mechanics, and Astronomy*, 68, 239501

Yuan, W., Zhang, C., Chen, Y., & Ling, Z. 2022, in *Handbook of X-ray and Gamma-ray Astrophysics*, ed. C. Bambi & A. Sangangelo, 86

Zhang, W., Yuan, W., Ling, Z., et al. 2025a, *Science China Physics, Mechanics, and Astronomy*, 68, 219511

Zhang, Y.-Q., Xue, W.-C., Zhang, J.-P., et al. 2025b, *ApJ*, 987, L38

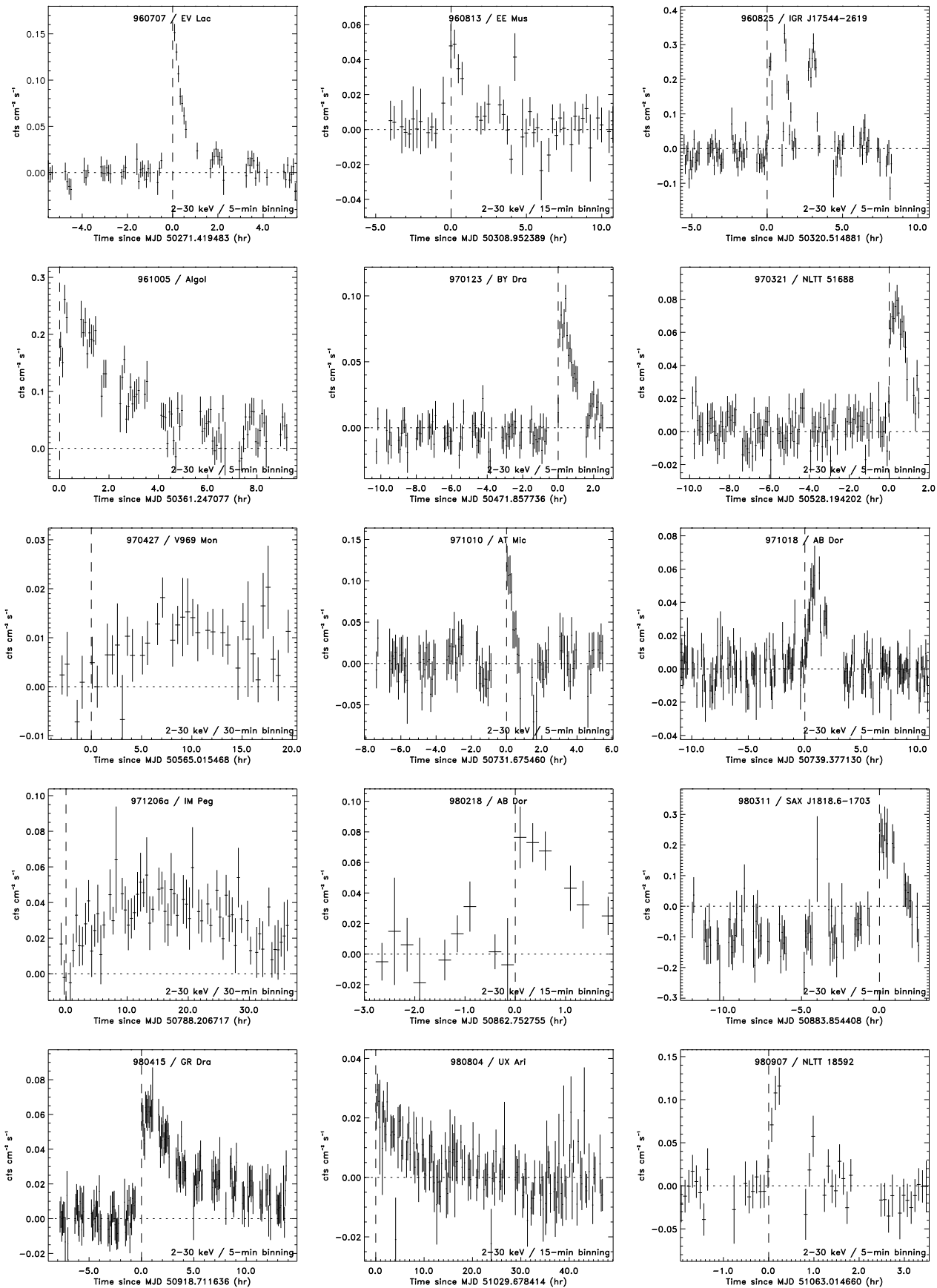


Fig. 3. Light curves of 49 flares from stars and HMXBs.

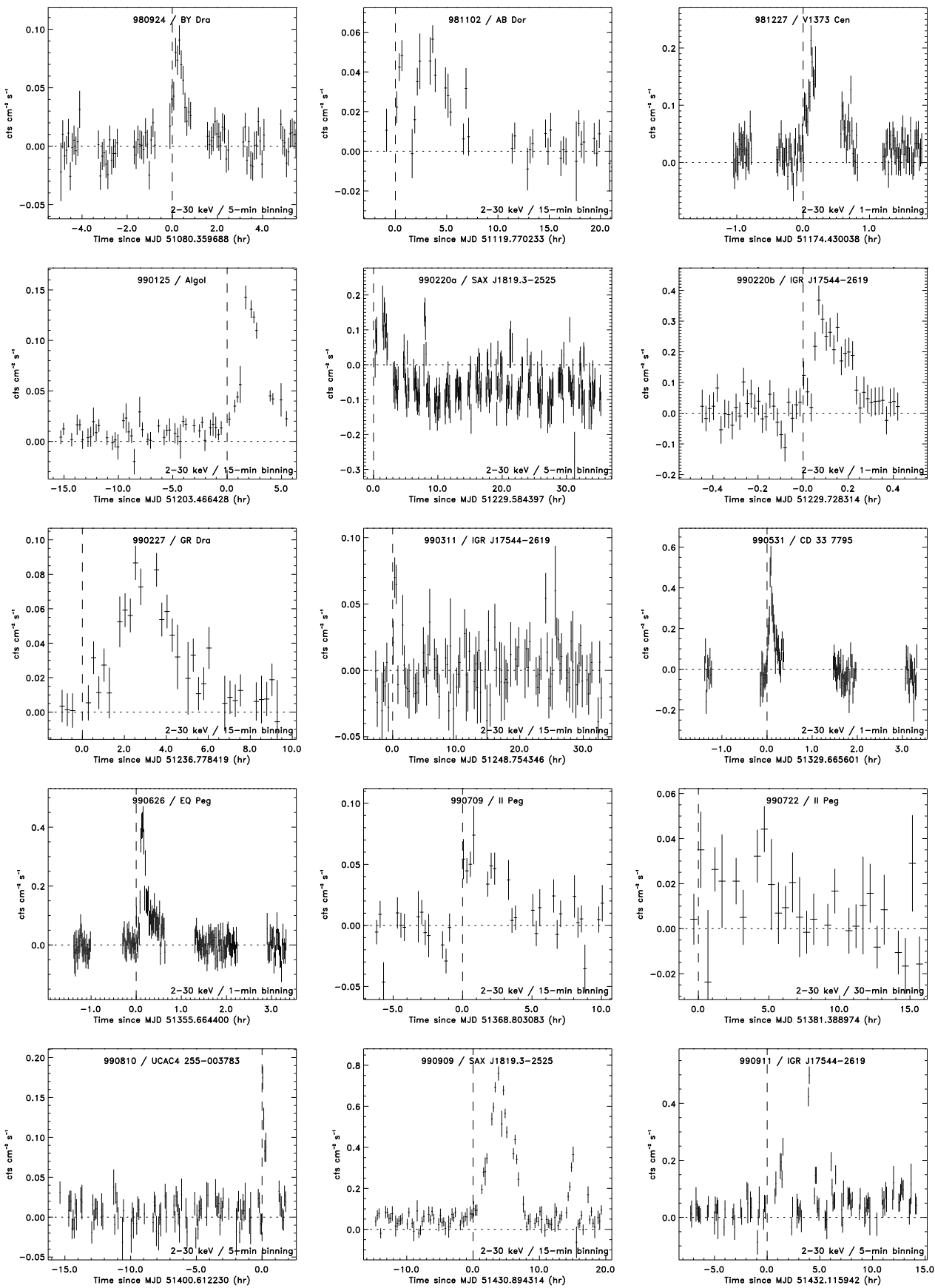


Fig. 3. cont'd (2/4)

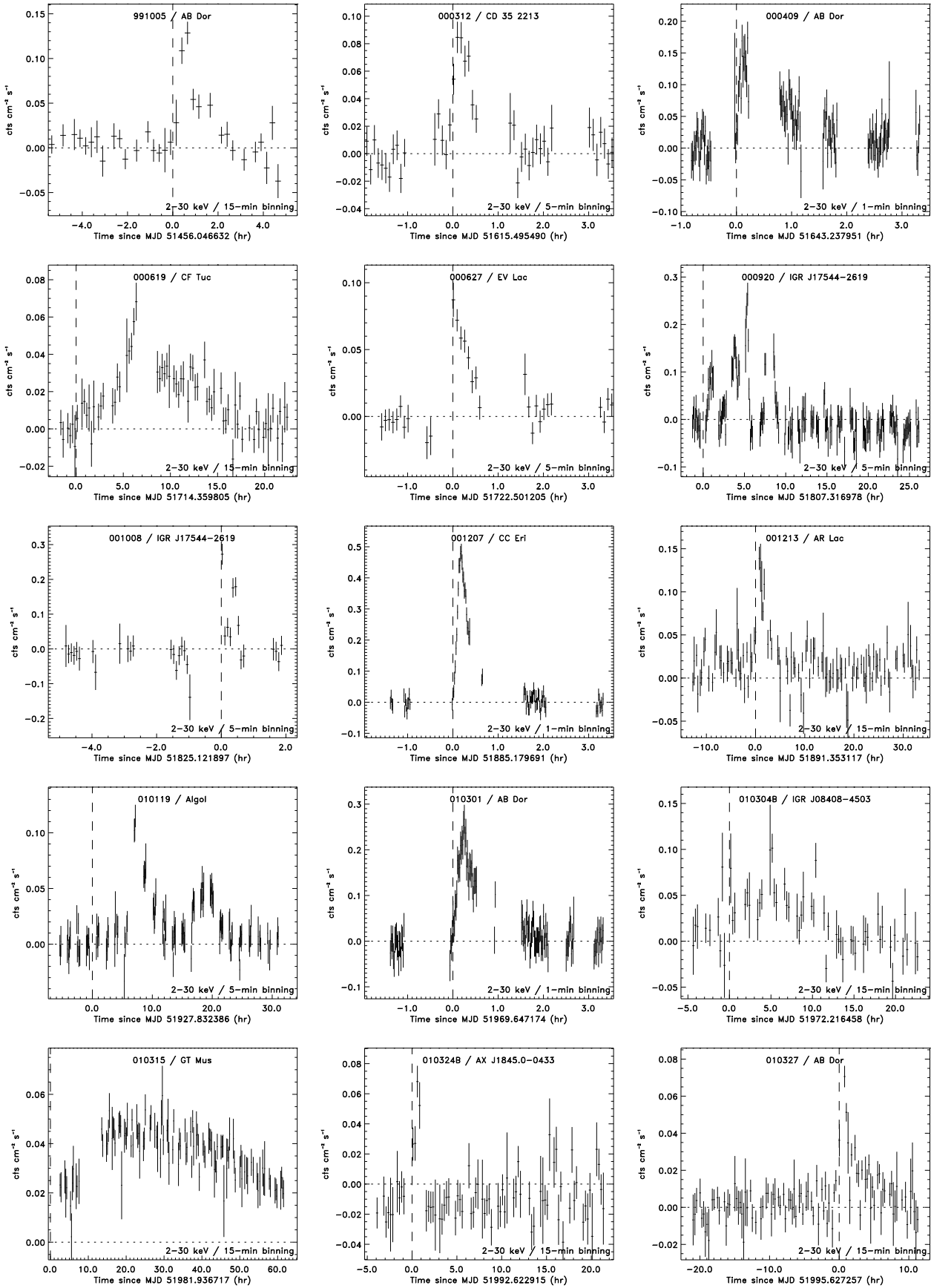
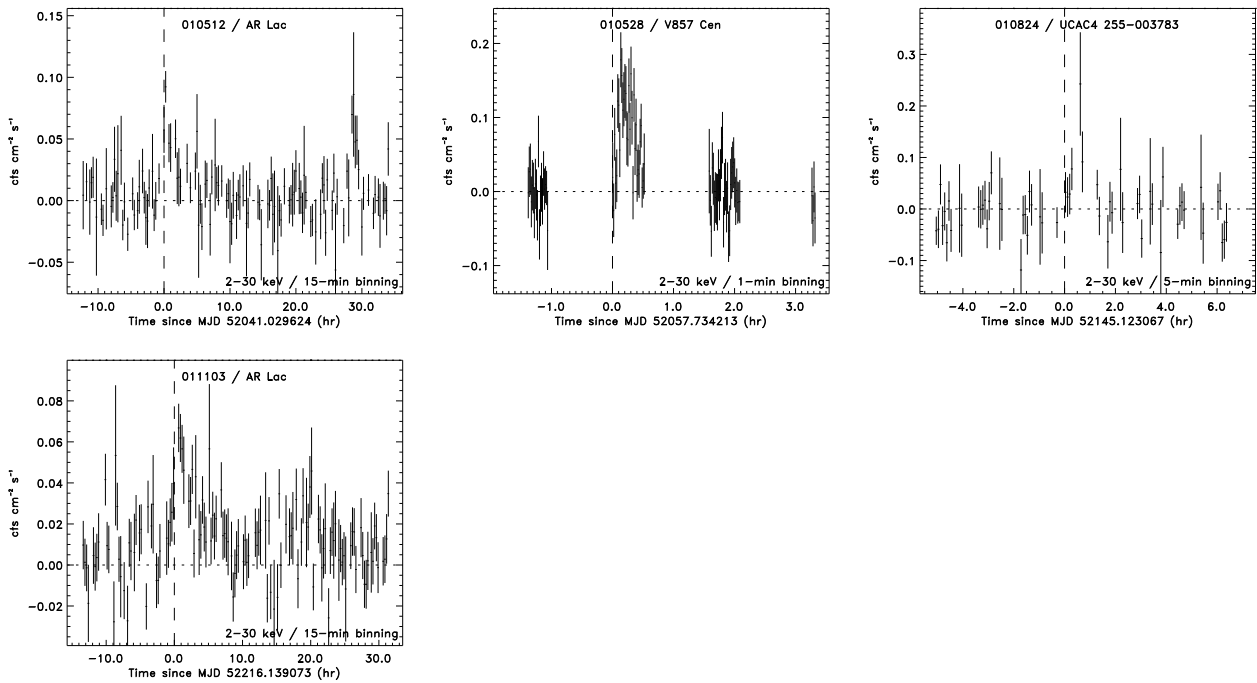


Fig. 3. cont'd (3/4)

**Fig. 3.** cont'd (4/4)

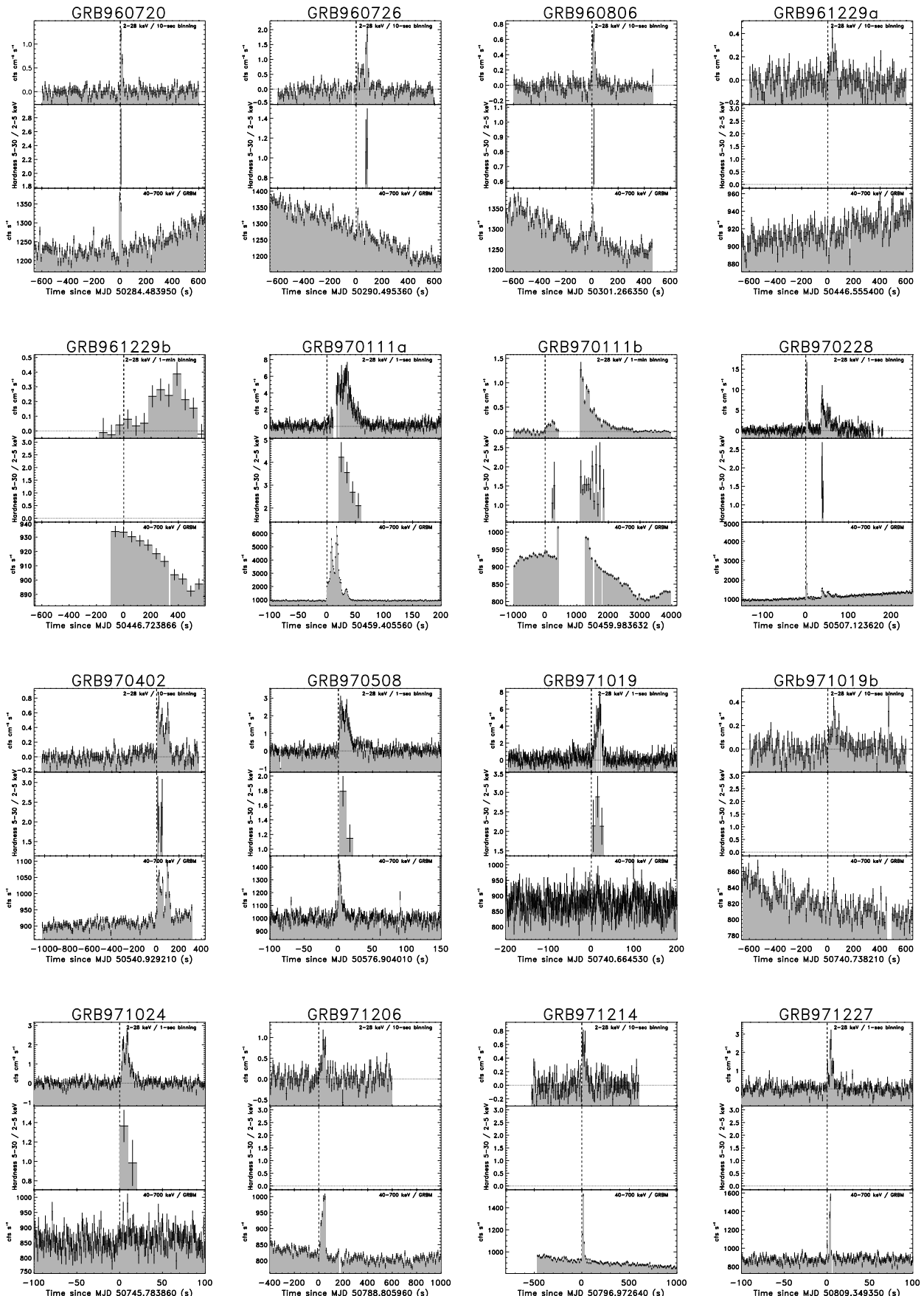


Fig. 4. Light curves of all 100 GRBs. Top panels: in WFC full bandpass (2-30 keV). Middle panels: 2-5/5-10 keV spectral softness ratio from WFC data. Bottom panels: 40-700 keV GRBM light curves. (1/7)

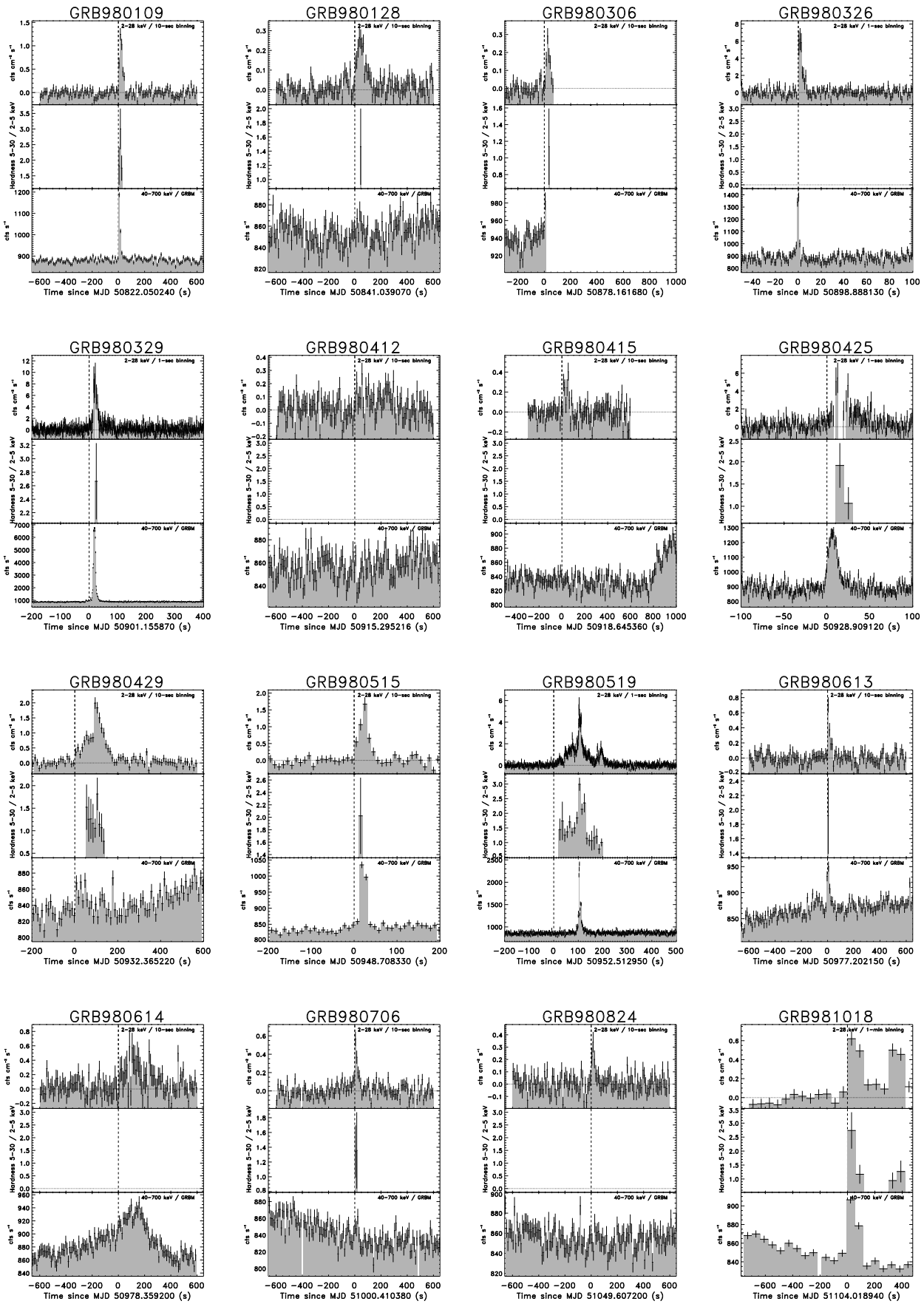


Fig. 4. cont'd (2/7)

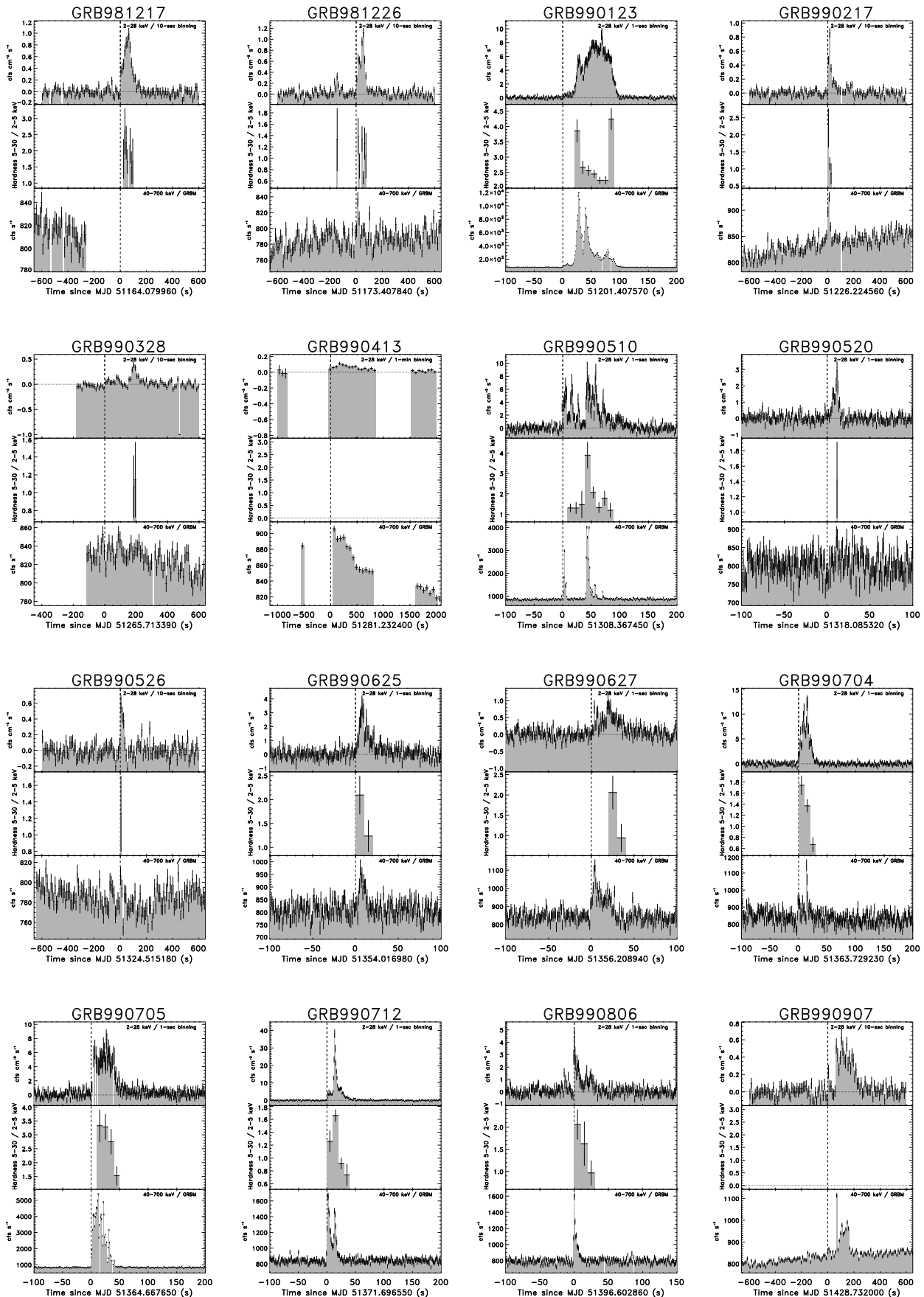


Fig. 4. cont'd (3/7)

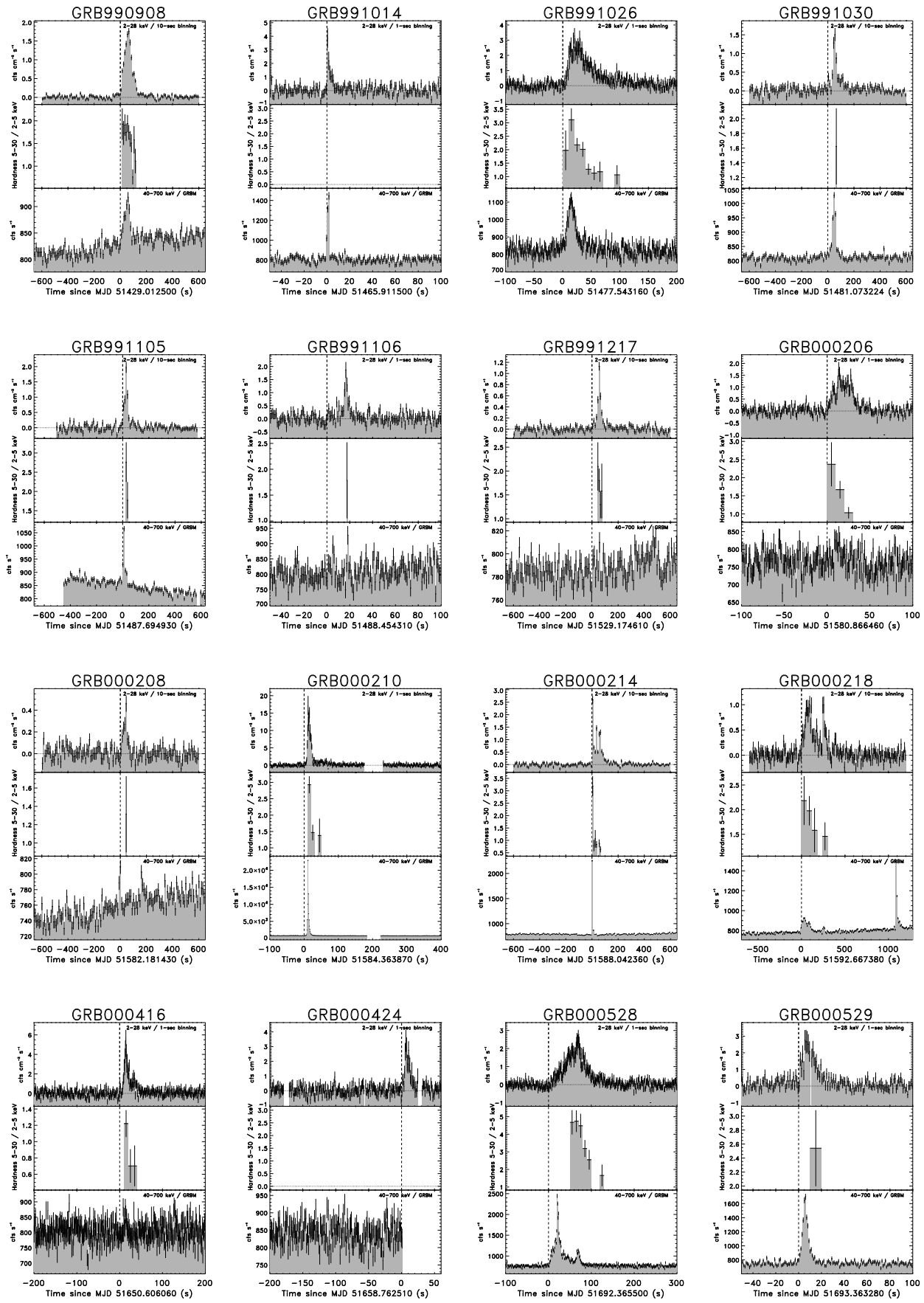


Fig. 4. cont'd (4/7)

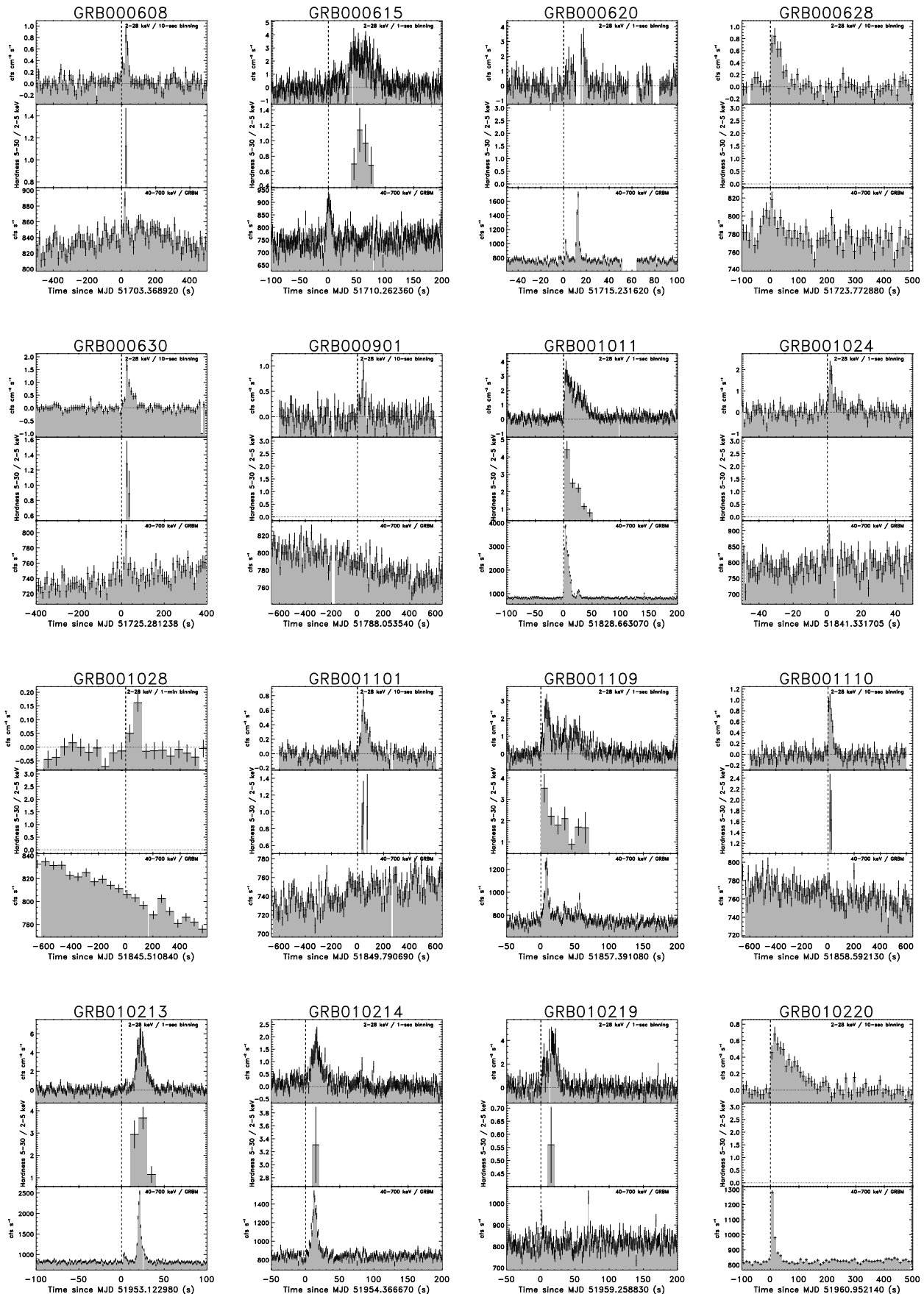


Fig. 4. cont'd (5/7)

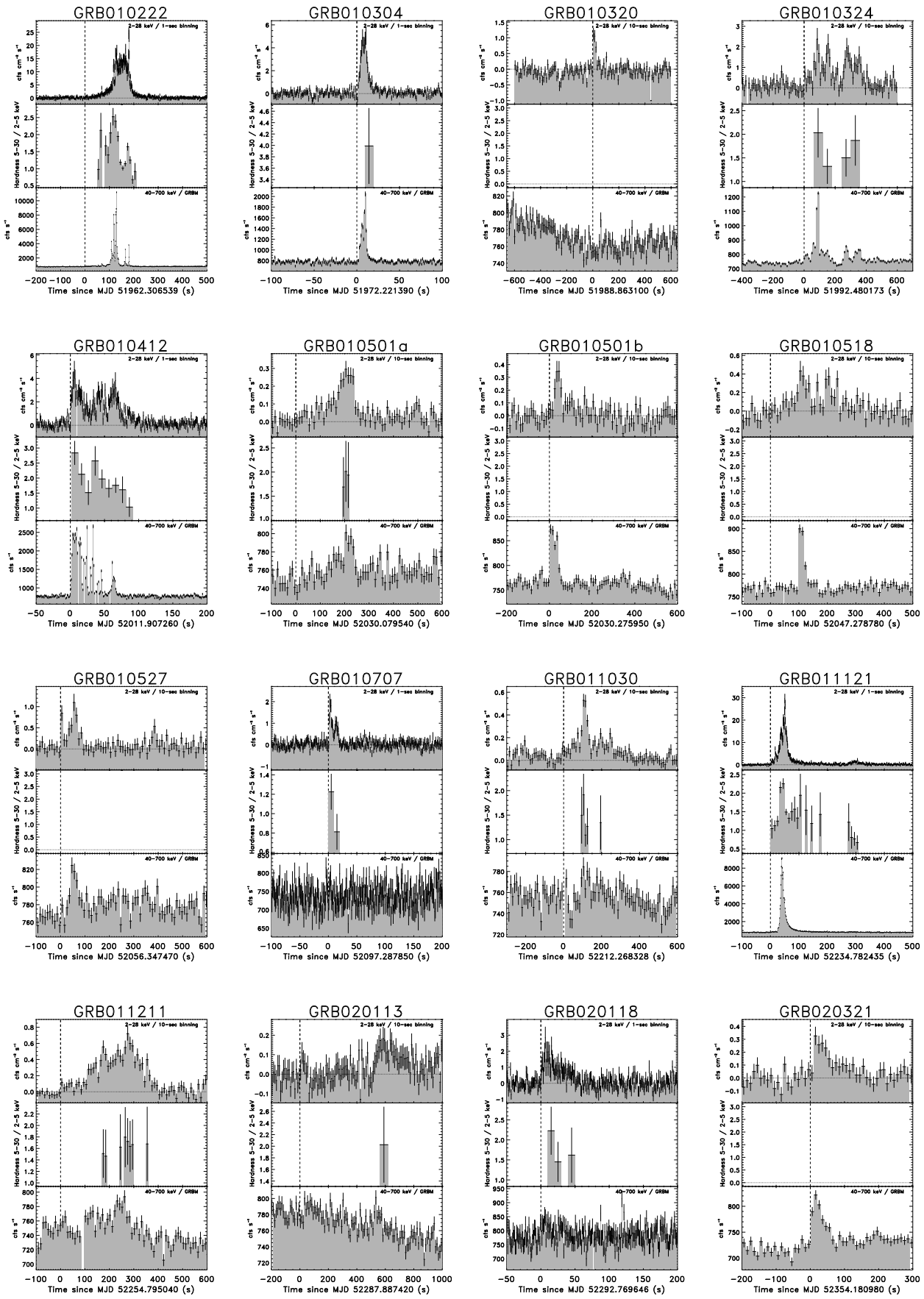


Fig. 4. cont'd (6/7)

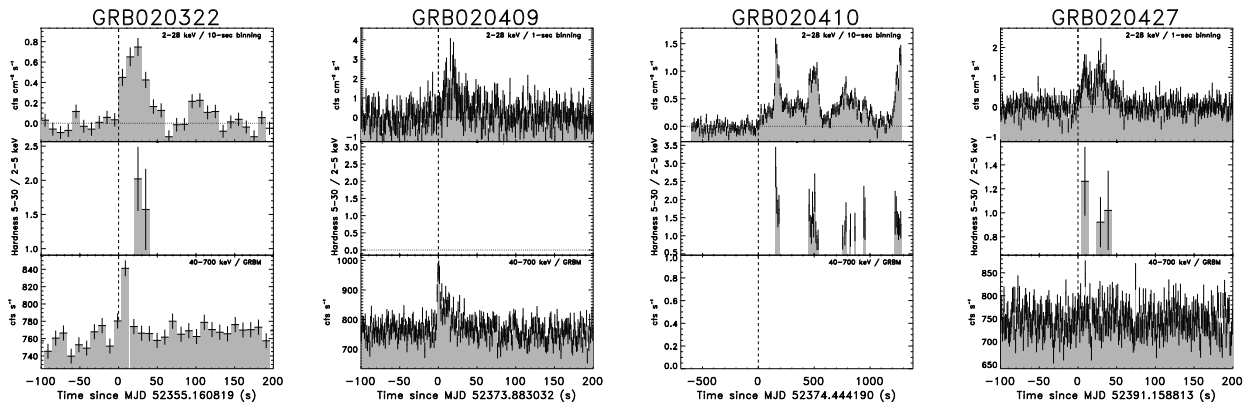


Fig. 4. cont'd (7/7)

Table 1. Catalog of 149 FXTs detected with BeppoSAX-WFC. For an explanation of this table, see Sect. 5 of main text.

ID	Ref [†]	r	OP/ WFC unit	MJD(UTC)-start	Duration (s)	Timescale		R.A.	Dec.	Err. ($''$)	Dev. ($''$)	BATSE ID	WFC/GRBM peak flux	Softness ratio	Type	Identification / remarks
						rise (s)	τ (min)									
960707	u		616/1	50271.419483	1 h	<30	41.8±3.4	341.7196	+44.3296	1.68	0.64		0.152		Flare star	EV Lac flare 1 / M-dwarf flare star with superflares (ref42)
960720	1	x	675/1	50284.483950	23(6)		0.148±0.027	262.6197	+49.0970	2.64		5545	1.21 / 1220	1.0	GRB	GRB970720 / First WFC GRB published, too large error reg for follow up
960726	u		689/2	50290.495360	150(5)		1.25±0.17	208.8450	-52.4484	2.74			1.81 / 190		GRB	GRB960726
960806	u		735/1	50301.266350	60(5)		0.246±0.043	32.6648	-0.6359	2.91			0.65 / 155		GRB	GRB960806
960813	u		757/2	50308.952389	2 h	<40	85.0±20.1	187.8133	-65.8235	3.15	2.49		0.049		Flare star	EE Mus=1RXS J123052.5-655020
960825	2		820/2	50320.514881	3.5 h			268.6070	-26.3305	1.70	0.27		0.332		SFXT	IGR J17544-2619 flare 1 / SFXT
961005	u		1075/2	50361.247077	5 h	?	175.7±11.5	47.0574	+40.9467	1.67	0.88		0.262		Flare star	Algol flare 1 / Flare star in a binary with an early-type star
961229a	u		1448/2	50446.555400	80(10)		0.417±0.178	224.7979	+18.5786	6.02			0.36 / <20	>18	GRB?	GRB961229a / XRF coincident with BD +19 2895 (K0 star)?
961229b	3		1448/1	50446.723866	300(50)		2	38.7055	-0.8724	3.31			0.39 / <20	>20.0	GRB?	GRB961229b / XRF coincident with PKS J0234-0049 (RADIO GALAXY)
970111a	4	+	1485/2	50459.405560	70(5)		0.348±0.019	232.0354	+19.5933	1.74			6.60 / 5800	1.1	GRB	GRB970111 / First GRB with follow up
970111b	3		1487/1	50459.983632	2500(100)	<18	6.55±0.26	86.1699	-40.7063	1.56			1.27 / 90	14	GRB	GRB970111b / Long GRB
970123	u		1565/2	50471.857736	3 h	7	61.9±6.9	278.4714	+51.7236	1.91	0.26		0.098		Flare star	BY Dra flare 1 / M-dwarf flare star
970228	5	+	1671/1	50507.123620	110(10)		0.511±0.057	75.4315	+11.7859	1.78	0.81		15.01 / 3900	3.8	GRB	GRB970228 / First GRB with successful follow up and distance
970321	u		1780/1	50528.194202	2 h	2	82.9±17.7	326.4788	-85.7153	1.73	0.87		0.079		Flare star?	NLTT 51688=1RXS J214641.1-854303 / M3.5 star with no known flare activity
970402	6	+	1830/1	50540.928920	130(10)		0.98±0.16	222.6150	-69.3224	4.66			0.75 / 160		GRB	GRB970402
970427	u		1930/2	50565.015468	20 h	300	1108.8±547.2	99.2513	-5.3676	2.82	1.33		0.018		RS CVn	V969 Mon=1RXS J063656.7-052104 / Faintest detected flare
970508	7	+	1984/2	50576.904030	120(10)		0.230±0.016	103.4250	+79.2696	1.94		6225	2.71 / 410	6.6	GRB	GRB970508 / First GRB with radio scintillation and evidence for beaming
971010	u		2622/2	50731.675460	0.5 h	<50	18.4±3.7	310.4521	-32.4547	3.75	1.51		0.117		Flare star	AT Mic / dwarf M flare star
971018	u		2699/2	50739.377130	3 h	30	82.8±13.2	82.1835	-65.4403	2.22	0.62		0.057		T Tau star	AB Dor flare 1

Table 1. continued.

ID	Ref [†]	r	OP/ WFC unit	MJD(UTC)-start	Duration (s)	Timescale rise (s)	τ (min)	R.A.	Dec.	Err. ($''$)	Dev. ($''$)	BATSE ID	WFC/GRBM peak flux	Softness ratio	Type	Identification / remarks
971019a	8	2705/2	50740.664410	30(2)		0.394±0.057	217.6194	+74.3645	2.56			untr	6.09 / 55	111	GRB	GRB971019a / XRF
971019b	u	2706/1	50740.738210	200(10)		0.844±0.211	88.9121	-74.9495	3.61				0.36 / 35	10	GRB	GRB971019b
971024	a	2732/1	50745.783860	23(3)		0.063±0.008	140.6739	+51.3087	2.04			untr	2.46 / 60	41	GRB	GRB971024 / XRR
971206a	u	3066/2	50788.206717	10 h	600	1252.8±316.8	343.2672	+16.8327	1.89	0.46			0.042		RS CVn	IM Peg
971206b	9	3066/1	50788.805960	60(5)		0.37±0.12	161.0457	-5.7792	4.44			6521	0.94 / 180	5.2	GRB	GRB971206
971214	10	+	3123/1	50796.972640	110(5)	0.31±0.10	179.1035	+65.1916	4.06	0.54		6533	0.64 / 585	1.1	GRB	GRB971214
971227	11	+	3205/2	50809.349350	12(2)	0.126±0.030	194.4174	+59.2444	3.70			6546	2.69 / 650	4.1	GRB	GRB971227
980109	12	x	3289/2	50822.050240	50(5)	0.185±0.033	6.5210	-63.0221	2.29			6564	1.25 / 285	4.4	GRB	GRB980109 / No afterglow found (no NFI)
980128	8	3465/2	50841.039070	160(10)		0.840±0.150	15.9980	+58.5142	2.78			untr	0.26 / <20	>13	GRB	GRB980128 / XRR
980218	u	3714/1	50862.752755	2 h	24	57.7±21.7	82.1791	-65.4693	3.09	1.13			0.076		T Tau star	AB Dor flare 2
980306	a	3875/2	50878.161680	50(?)		0.339±0.075	240.8666	-77.8760	2.91			untr	0.30 / 35	8.4	GRB	GRB980306 / XRR
980311	13	3905/2	50883.855408	2 h	<40	119.9±20.0	274.7542	-16.9006	5.00			10.57	0.269		SFXT	SAX J1818.6-1703
980326	14	x	4057/1	50898.888130	9(1)	0.036±0.008	129.1306	-18.8800	3.19	1.56		6660	6.22 / 480	13	GRB	GRB980326
980329	15	+	4073/2	50901.155870	90(5)	0.286±0.048	105.6408	+38.8432	3.22	0.84		6665	9.29 / 6345	1.5	GRB	GRB980329
980412	u	4169/2	50915.295216	300(30)	4	0.80±0.42	123.0199	-49.5219	4.74				0.27 / <20	>14	GRB?	GRB980412 / XRF, coincides with HD 6881 (K3(III) star)
980415	u	4202/2	50918.645360	60(10)	0.8	0.105±0.064	246.6110	+63.5242	5.00				0.29 / <20	>14	GRB?	GRB980415 / XRF
980415b	u	4202/2	50918.711636	15 h	<35	409.0±28.8	262.1440	+59.0247	1.64	0.89			0.061		High-E transient?	GRB Dra flare 1 / See also 990227
980425	16	+	4281/2	50928.909030	80(5)	0.5	0.378±0.052	293.7303	-52.8553	2.63	1.31	6707	6.34 / 400	16	GRB	GRB980425=SN1998bw / first supernova Ic association
980429	17	+	4320/2	50932.365870	180(10)	2	0.656±0.056	130.1491	+22.8360	1.92			1.99 / 35	57	GRB	GRB980429 / XRF
980515	18	+	4462/2	50948.708330	200(10)	0.3	0.164±0.028	319.3480	-67.2500	2.63			1.67 / 185	9.0	GRB	GRB980515 / no counterpart found in other wavelengths than X-rays
980519	19	+	4480/2	50952.512600	165(4)	3.5	0.215±0.021	350.5923	+77.2505	1.53	0.69	6764	6.15 / 1515	4.1	GRB	GRB980519 / very soft prompt black body X-ray spectrum
980613	9	+	4677/2	50977.202150	40(3)	0.1	0.246±0.056	154.4848	+71.4853	3.42	1.68		0.71 / 85	8.3	GRB	GRB980613
980614	u	4683/1	50978.359433	600(60)			337.7366	+33.3625	5.00				0.57 / <0.02	>29	GRB?	GRB980614
980706	u	4894/2	51000.410380	300(60)	3	0.325±0.065	193.1647	+28.0604	3.19				0.57 / <20	>38	GRB?	GRB980706
980804	u	5072/2	51029.678414	72000	?	951.8±96.5	51.6457	+28.6986	2.39	1.07			0.029		RS CVn	UX Ari / Very long stellar flare
980824	u	5166/2	51049.607200	70(10)	0.5	0.48±0.18	268.3526	+48.5036	4.24				0.34 / <20	>17	GRB?	GRB980424 / XRF
980907	u	5275/1	51063.014660	2 h	1	45.6±11.4	117.2305	-76.6945	2.45	1.13			0.116		Flare star	NLTT18592=2RE J074922-764149 / dMe star; 555 TESS flares (ref43)
980924	u	5385/1	51080.359688	1 h	6	30.0±5.3	278.5036	+51.7251	2.35	0.94			0.091		Flare star	BY Dra flare 2 / M-dwarf flare star
981018	3	5618/2	51104.017550	700(50)	1	undet	110.2276	+1.0364	2.11			untr	0.62 / 35	18	GRB	GRB981018
981102	u	5745/1	51119.770233	9 h	20	433.4±66.2	82.1867	-65.4456	2.20	0.30			0.057		T Tau star	AB Dor flare 3

Table 1. continued.

ID	Ref [†]	r	OP/ WFC unit	MJD(UTC)-start	Duration (s)	Timescale rise (s)	τ (min)	R.A.	Dec.	Err. ($''$)	Dev. ($''$)	BATSE ID	WFC/GRBM peak flux	Softness ratio	Type	Identification / remarks	
981217	9	6002/2	51164.079960	150(10)	1.5	0.493±0.057	294.6259	+80.5517	1.95				0.98 / n.a.		GRB?	GRB981217	
981226	20	+	6055/1	51173.407840	260(5)	1	0.416±0.037	352.4125	-23.9166	1.81			1.12 / 60	19	GRB	GRB981226 / XRF	
981227	u		6069/2	51174.430038	1 h	12	25.6±2.9	175.1515	-62.0102	2.18	1.37		0.213 / 50	4.3	Flare star	V1373 Cen=1RXS J114028.6-620142 / BY Dra type star	
ratio 990123	21	+	6221/1	51201.407570	100(5)	0.2	undet	231.3719	+44.7483	1.44	1.11	7343	9.39 / 11200	0.8	GRB	GRB990123 / 2nd brightest in GRBM	
990125	u		6231/2	51203.466428	6 h	25	107.7±8.5	47.0381	+40.9607	1.64	0.36		0.148		Flare star	Algol 2 / flaring K star in a binary with an early-type star (ref44)	
990217	9	+	6383/2	51226.224560	80(5)	0.1	0.243±0.031	45.7130	-53.0933	2.31			0.86 / 85		10	GRB	GRB990217
990220a	22		6419/1	51229.584397	30h			274.8431	-25.4646	4.23	3.84		0.161		HMXB	SAX J1819.3-2525 flare 3	
990220b	23		6419/1	51229.728314	0.2 h	1	10	268.6071	-26.3230	2.13	0.19		0.368		SFXT	IGR J17544-2619 flare 2	
990227	u		6473/2	51236.778419	6 h	120	142.1±17.3	262.1621	+59.0221	1.93	0.79		0.083		High-E transient?	GR Dra flare 2 / G0 star unknown as flare star, possibly GRO J1753+57 (gamma-ray flarer). See also 980415b	
990311	23		6570/1	51248.754346	1h			268.5934	-26.3139	3.80	1.04		0.070		SFXT	IGR J17544-2619 flare 6	
990328	u		6742/1	51265.715390	260(10)	3	0.480±0.097	136.5108	-54.9291	2.84			0.39 / <20	>19	GRB?	GRB990328 / XRF	
990413	3		6829/2	51281.232860	1000(200)	<20	10.6±2.7	160.1040	+81.8236	2.54			0.11 / 60	1.8	GRB	GRB990413 / long GRB	
990510	24	+	6902/2	51308.367430	120(5)	0.5	0.463±0.026	204.5196	-80.4961	1.60	0.11	7560	8.62 / 3105	2.8	GRB	GRB990510 / bright in WFC	
990520	8	+	6952/1	51318.085320	21(2)	2	0.016±0.012	128.9784	+51.3096	2.99			2.95 / <80	>37	GRB	GRB990520 / XRF	
990526	a		6975/1	51324.515180	32(2)	0.1	0.24±0.07	155.6031	-62.7798	3.09			0.59 / 25	24	GRB	GRB990526 / XRF	
990531	u		6990/1	51329.665601	0.5 h	4	19.7±4.9	172.9817	-34.6066	2.16	0.10		0.533		T Tau star	CD-33 7795=1RXS J113155.7-343632 / 32 flares seen with TESS (Ref45)	
990625	25	x	7072/2	51354.016980	38(7)	0.1	0.273±0.034	6.6877	-31.2028	2.68			3.50 / 175	20	GRB	GRB990625 / too large initial error box for follow up	
990626	u		7088/2	51355.664400	1 h	1	10.2±0.7	352.9638	+19.9369	1.90	0.27		0.427		Flare star	EQ Peg / M-dwarf flare star with superflares	
990627	26	+	7096/2	51356.208940	90(3)	0.5	0.239±0.036	27.1347	-77.0958	2.32			0.96 / 300	3.2	GRB	GRB990627	
990704	27	+	7141/1	51363.729230	40(2)	0.3	0.086±0.006	184.8717	-3.8021	1.90			12.48 / 310	40	GRB	GRB990704 / XRF	
990705	28	+	7147/2	51364.667650	150(10)	0.5	0.246±0.020	77.4676	-72.1307	1.78	0.28		6.65 / 4720	1.4	GRB	GRB990705	
990709	u		7167/1	51368.803083	4 h	<50	204.5±44.6	358.7690	+28.6291	2.74			0.074		RS CVn	II Peg flare 1	
990712	29	x	7188/2	51371.696550	60(5)	0.1	0.149±0.005	337.9701	-73.4058	1.50	0.12		38.22 / 820	47	GRB	GRB990712 / Brightest WFC GRB	
990722	u		7263/2	51381.388974	5 h	~100	421.9±132.5	358.7840	+28.6111	4.82	1.91		0.044		RS CVn	II Peg flare 2	
990806	30	+	7348/1	51396.602510	60(5)	0.5	0.238±0.028	47.6466	-68.1245	2.13		7701	4.28 / 785	5.5	GRB	GRB990806	

Table 1. continued.

ID	Ref [†]	r	OP/ WFC unit	MJD(UTC)-start	Duration (s)	Timescale rise (s)	τ (min)	R.A.	Dec.	Err. ($''$)	Dev. ($''$)	BATSE ID	WFC/GRBM peak flux	Softness ratio	Type	Identification / remarks
990810	u	7362/2	51400.612230	1 h	1	16.4±3.8		56.6564	-39.1073	2.17	0.37		0.174		T Tauri?	SAX J0346.6-3906=UCAC4 255-003783? / This is a 16 mag 3700K star (see also 010824)
990907	9	+	7523/2	51428.732000	250(10)	0.2	1.37±0.15	112.6887	-69.4057	1.99		7755	0.63 / 275	2.3	GRB	GRB990907
990908	9	x	7523/2	51429.012500	160(5)	1	0.615±0.024	103.4133	-75.0104	1.50			1.76 / 90	20	GRB	GRB990908
990909	22		7546/2	51430.894314	17h			274.8459	-25.3962				0.760		HXMB	SAX J1819.3-2525 flare 2
990911	u	7553/1	51432.115942	>15h				268.6409	-26.3300	1.97	1.83		0.499		SFXT	IGR J17544-2619 flare 3
991005	u	7692/2	51456.046632	3 h	2	58.2±8.8		82.1773	-65.4560	2.25	0.38		0.129		T Tau star	AB Dor flare 4
991014	31	+	7749/2	51465.911500	11(2)	0.1	0.044±0.009	102.7685	+11.5979	3.75		7803	3.88 / 620	6.3	GRB	GRB991014
991026	9		7820/2	51477.543160	300(10)	0.5	0.605±0.032	248.7926	-89.5048	1.65			3.28 / 315	10	GRB	GRB991026
991030	9		7840/2	51481.073455	120(10)	0.5	0.400±0.058	122.5798	-48.4265	2.40			1.49 / 230	6.5	GRB	GRB991030
991105	9	x	7859/2	51487.694720	150(5)	0.8	0.153±0.026	180.8616	-66.7735	2.12		7841	1.98 / 215	9.2	GRB	GRB991105
991106	9	+	7860/1	51488.454310	10(2)	0.3	0.038±0.008	336.2170	+54.3647	3.21			3.67 / 110	33	GRB	GRB991106 / XRR
991217	32	x	8073/2	51529.174610	120(20)	0.8	0.264±0.024	345.8144	+0.2494	4.5			1.13 / <20	>57	GRB?	GRB991217
000206	33		8374/1	51580.866460	60(5)	0.1	0.251±0.023	226.4360	+72.1146	1.86		untr	1.75 / 50	35	GRB	GRB000206 / XRR
000208	a		8386/1	51582.181370	70(5)	0.5	0.199±0.066	28.9025	-22.8470	3.62		untr	0.44 / 50	8.9	GRB	GRB000208 / XRR
000210	34	+	8406/1	51584.363870	80(5)	0.1	0.133±0.007	29.8032	-40.6742	1.77	1.05		17.17 / 20710	0.8	GRB	GRB990210 / Brightest GRBM GRB
000214	35	+	8425/1	51588.042360	120(5)	0.1	0.438±0.039	283.5719	-66.4414	1.62			2.59 / 1825	1.4	GRB	GRB000214
000218	u		8468/2	51592.667380	450(30)	<1	3.70±0.35	114.4409	-71.3064	1.93			0.98 / 185	5.3	GRB	GRB000218
000312	u		8683/2	51615.49454	0.6 h	1	24.0±4.3	79.3413	-35.3630	2.20	0.27		0.085		Flare star	CD-35 2213=2RE J051724-352221 / dMe star). 110 flares with TESS (Ref34)
000409	u		8881/1	51643.237951	1.5 h	2	60.5±6.2	82.1924	-65.4477	2.05	0.24				T Tau star	AB Dor flare 5
000416	9	x	8942/2	51650.606060	80(5)	0.1	0.220±0.020	258.8558	-71.6100	2.27		untr	5.69 / 85	67	GRB	GRB000416 / XRF
000424	9	x	9004/2	51658.762510	50(?)	0.1	0.394±0.115	104.7273	+49.8753	2.44		8086	3.39 / n.a.		GRB	GRB000424
000528	9	+	9145/2	51692.365500	170(5)	1	0.441±0.022	161.2791	-33.9859	1.60			2.65 / 1615	1.6	GRB	GRB000528
000529	9	+	9153/2	51693.363180	70(5)	0.3	0.151±0.020	2.3505	-61.5298	2.46			3.15 / 860	3.7	GRB	GRB000529
000608	9	x	9232/2	51703.368920	50(5)	0.3	0.144±0.039	6.2623	-69.0416	3.28			0.84 / 50	17	GRB	GRB000608
000615	9	+	9251/1	51710.262360	90(5)	0.7	0.523±0.058	233.1700	73.8184	2.01			3.49 / 160	22	GRB	GRB000615 / XRF
000619	u		9275/1	51714.359805	10 h	360	355.1±55.0	13.2643	-74.6457	1.86	0.38		0.068		RS CVn	CF Tuc
000620	9	x	9275/2	51715.231620	30(5)	0.2	0.076±0.017	113.8024	+69.1922				3.53 / 895	3.9	GRB	GRB000620
000627	u		9331/1	51722.501215	0.6 h	<30	25.2±5.2	341.7074	+44.3234	2.33	1.17		0.087		Flare star	EV Lac 2 / M-dwarf flare stars with superflares (Ref32)
000628	u		9341/2	51723.772880	70(5)	0.1	0.553±0.103	236.1639	-69.7477	2.82			0.84 / 50	17	GRB	GRB000628
000630	u		9352/1	51725.281238	100(10)	0.2	0.357±0.062	233.8921	+57.8930	2.82			1.65 / 75	22	GRB	GRB000630
000901	u		9696/2	51788.053540	100(10)	0.8	0.535±0.189	268.6004	-26.3313	4.4			0.91 / <20	>46	GRB?	'GRB000901' / XRF, coincides with EQ J084834.9-785352 / M5 star (unknown as flare star). (Ref35)

Table 1. continued.

ID	Ref [†]	r	OP/ WFC unit	MJD(UTC)-start	Duration (s)	Timescale rise (s)	τ (min)	R.A.	Dec.	Err. ($''$)	Dev. ($''$)	BATSE ID	WFC/GRBM peak flux	Softness ratio	Type	Identification / remarks	
000920	23	9832/2	51807.316978	9h				268.6704	-26.3206	1.87	3.42		0.263		SFXT	IGR J17544-2619 flare 4	
001008	23	9934/2	51825.121897	35min				268.6704	-26.3206	2.72	0.48		0.272		SFXT	IGR J17544-2619 flare 5	
001011	9	x	9957/2	51828.663080	65(5)	0.5	0.446 \pm 0.019	275.7687	-50.8999	1.56	0.53		3.60 / 3005	1.2	GRB	GRB001011	
001024	u		10050/1	51841.331705	30(5)	0.1	0.057 \pm 0.017	125.5960	-87.7158	3.80			1.96 / 105	19	GRB	GRB001024 / XRF	
001028	u		10055/2	51845.510840	130(10)	1.2	0.632 \pm 0.281	173.2039	-86.1883	5.40			0.16 / <50	>3.3	GRB?	GRB001028 / XRF	
001101	u		10091/1	51849.790690	200(10)	0.8	0.644 \pm 0.086	123.1415	+48.2890	2.27			0.74 / <10	>74	GRB?	GRB001101	
001109	9	+	10146/1	51857.391080	120(5)	0.2	0.689 \pm 0.051	277.5242	+55.3079	1.84			2.86 / 460	6.2	GRB	GRB001109	
001110	u		10159/2	51858.592130	100(10)	0.2	0.496 \pm 0.067	300.6197	-20.5037	2.56			0.97 / <20	>48	GRB?	GRB001110 / XRF	
001207	u		10302/1	51885.179691	1 h	12	19.4 \pm 1.2	38.5894	-43.7960	1.46	0.27		0.485		Flare star	CC Eri, brightest stellar flare	
001213	u		10320/2	51891.353117	4 h	40	86.5 \pm 14.8	332.1754	+45.7434	2.20	0.21		0.139		RS CVn	AR Lac flare 1	
010119	u		10570/1	51927.832386	22h	<60		47.0529	+40.9608	1.83	0.58		0.115		Flare star	Algol flare 3 / K-type flaring star in a binary with an early-type star	
010213	a		10725/2	51953.122980	40(5)	0.3	0.143 \pm 0.011	257.3390	+39.2681	1.93			5.80 / 1550	3.7	GRB	GRB010213 / XRF	
010214	36	+	10727/2	51954.366670	60(5)	0.3	0.184 \pm 0.024	265.2453	48.5508	2.25			1.98 / 655	3.0	GRB	GRB010214	
010219	u		10747/1	51959.258830	45(3)	0.4	0.09 \pm 0.018	94.1820	-69.7800	2.26			4.10 / 160	26	GRB	GRB010219	
010220	9	+	10753/2	51960.952140	200(10)	0.1	1.21 \pm 0.12	39.2459	+61.7612	1.97			0.66 / 455	1.5	GRB	GRB010220	
010222	37	+	10767/1	51962.306539	300(20)	3	0.494 \pm 0.048	223.0499	+43.0130	1.46	0.34		24.53 / 9840	2.5	GRB	GRB010222	
010301	u		10800/1	51969.647174	8 h	20	37.4 \pm 5.0	82.1948	-65.4533	1.68	0.28		0.267		T Tau star	AB Dor flare 6	
010304	9		10822/2	51972.221380	40(5)	0.1	0.200 \pm 0.018	316.5876	+53.2077				4.99 / 1225	4.1	GRB	GRB010324	
010304b	u		10822/1	51972.42479	~15h				130.2049	-45.0477	2.76	0.69		0.101		SFXT	IGR J08408-4503
010315	u		10883/1	51981.336717	60 h	800	4200	175.0108	-65.3811	1.55	3.55		0.064		RS CVn	GT Mus	
010320	u		10923/1	51988.863100	60(5)	0.5	0.456 \pm 0.084	277.1368	-10.6302	2.84			1.12 / <30	>37	GRB?	GRB010320	
010324a	38		10954/1	51992.480173	420(30)	6	1.63 \pm 0.35	107.8541	+19.9954	2.43			2.38 / 510	4.7	GRB	GRB010324 / coincident with LEDA 1613994	
010324b	u		10954/2	51992.622915	1 h	30	15	282.5536	-4.5534	9.70	2.04		0.068		SFXT	AX J1845.0-0433	
010327	u		10972/1	51995.627257	2 h	<30	107.7 \pm 14.3	82.1861	-65.4506	2.32	0.01		0.071		T Tau star	AB Dor flare 7	
010412	9	x	11085/1	52011.907160	110(5)	1.2	0.244 \pm 0.025	294.9057	+13.6124	1.65			4.74 / 1860	2.5	GRB	GRB010412	
010501a	u		11203/2	52030.079540	300(60)	3	0.654 \pm 0.107	88.2420	+78.7952	2.31			0.30 / 60	4.9	GRB	GRB010501A	
010501B	9		11203/1	52030.275950	180(60)	0.5	0.690 \pm 0.161	286.7133	-70.1803	4.18			0.34 / 120	2.9	GRB	GRB010501B	
010512	u		11268/1	52041.02962	2 h	15	348.5 \pm 53.3	332.1789	+45.7261	3.42	0.98		0.092		RS CVn	AR Lac flare 2	
010518	9	x	11292/2	52047.278780	330(30)	1.7	1.80 \pm 0.40	161.6546	-57.7643	3.21			0.43 / 130	3.3	GRB	GRB010518	
010527	u		11324/2	52056.347470	75(5)	1.0	0.309 \pm 0.072	189.2384	+36.1791	3.01			1.10 / 65	17	GRB	GRB010527	
010528	39		11330/1	52057.734213	0.6 h	5	21.2 \pm 4.5	116.9450	-57.6173	2.41	0.51		0.178		Flare star	V857 Cen = Gl 431 / M dwarf flare star	
010707	9		11486/1	52097.287850	22(3)	0.1	0.129 \pm 0.016	205.5666	-38.5365	2.16			2.04 / <70	>29	GRB?	GRB010707 / XRF	
010824	u		11828/2	52145.123067	45min			56.6818	-39.1525	14.1869			0.243		T Tauri?	SAX J0346-3906 / see also 990810	
011030	9	x	12150/1	52212.268328	300(30)	2	1.54 \pm 0.16	310.9180	+77.2925	1.95	0.50		0.52 / 30	18	GRB	GRB011030 / XRR, first real time follow up X-ray flash	
011103	u		12167/2	52216.139073	3 h	15	116.1 \pm 26.2	332.1717	+45.6598	2.86	4.90		0.067		RS CVn	AR Lac flare 3	

Table 1. continued.

ID	Ref [†]	r	OP/ WFC unit	MJD(UTC)-start	Duration (s)	Timescale rise (s)	τ (min)	R.A.	Dec.	Err. ($''$)	Dev. ($''$)	BATSE ID	WFC/GRBM peak flux	Softness ratio	Type	Identification / remarks
011121	9	+	12252/1	52234.782435	400(30)	0.8	0.939±0.076	173.6086	-76.0259	1.45	0.26		29.64 / 7695	3.9	GRB	GRB011121 / 2nd brightest IN WFC / peak flux of first peak
011211	9	+	12361/1	52254.795040	700(30)	4.7	0.988±0.099	168.8179	-21.9368	1.70	0.83		0.72 / 50	14	GRB	GRB011211 / XRR
020113	u		12497/2	52287.887420	1000(100)	6	4.75±0.90	226.6594	+83.4713	4.12			0.18 / 35	5.2	GRB	GRB020113
020118	9		12513/2	52292.769646	50(10)	0.1	0.374±0.046	9.4460	+59.5364	2.27			2.85 / 60	47	GRB	GRB020118
020321	31	+	12705/1	52354.180980	150(20)	0.3	0.960±0.214	243.1410	-83.7157	3.31			0.31 / 100	3.1	GRB	GRB020321
020322	3	+	12712/2	52355.160819	120(10)	0.5	0.374±0.063	270.2379	+81.0880	2.47	1.21		0.75 / 80	9.4	GRB	GRB020322
020409	3	x	12830/1	52373.882928	90(10)	0.5	0.324±0.075	131.2984	+66.6810	3.75			3.24 / 210	15	GRB	GRB020409
020410	3	+	12830/2	52374.444190	>1300s	2.5	complicated	331.6779	-83.8217	1.52	0.34		1.46 / n.a.		GRB?	GRB020410 / XRR
020427	40,41	+	12933/2	52391.158859	65(5)	0.2	0.378±0.079	332.3803	-65.3276	2.22			1.90 / <100	>19	GRB?	GRB020427 / XRF, first coincidence of GRB with ionospheric event

[†]1 - Piro et al. (1998); 2 - in't Zand et al. (2004a); 3 - in't Zand et al. (2004b); 4 - Costa et al. (1997a); 5 - Costa et al. (1997b); 6 - Nicastro et al. (1998); 7 - Piro et al. (1998); 8 - Kippen et al. (2003); 9 - Vetere et al. (2007); 10 - Dal Fiume et al. (2000); 11 - Antonelli et al. (1999a); 12 - in't Zand et al. (1998b); 13 - in't Zand et al. (1998a); 14 - Celidonio et al. (1998); 15 - in't Zand et al. (1998b); 16 - Pian et al. (1999); 17 - Romano et al. (2008); 18 - Ricci et al. (1998); 19 - in't Zand et al. (1998b); 20 - Frontera et al. (2000); 21 - Corsi et al. (2005); 22 - in't Zand et al. (2000); 23 - in't Zand et al. (2004a); 24 - Kuulkers et al. (2000); 25 - Piro (1999); 26 - Antonelli et al. (1999b); 27 - Feroci et al. (2001); 28 - Amati et al. (2000); 29 - Frontera et al. (2001); 30 - Montanari et al. (2001); 31 - in't Zand et al. (2000); 32 - Muller et al. (1999); 33 - Heise et al. (2001); 34 - Piro et al. (2002); 35 - Antonelli et al. (2000); 36 - Guidorzi et al. (2003); 37 - in't Zand et al. (2001); 38 - Guidorzi et al. (2001); 39 - in't Zand et al. (2001); 40 - Amati et al. (2004); 41 - Fishman et al. (2002); 42 - Osten et al. (2010); 44 - van den Oord & Mewe (1989); 43 - Seli et al. (2025); 45 - Lawson et al. (2002);

Table 2. Spectral fits with a power law. No line was included in fit, except for events listed in Table 3. N_{H} was fixed at 0, except for events listed in Table 4. Distances were extracted from Simbad, redshift or via GAIA parallaxes.

ID	OP/ WFC	MJD-start	Time span (s)	Photon index	2-30 keV fluence (10 $^{-6}$ erg cm $^{-2}$)	χ^2_{r}	Distance (pc/z)	2-30 keV energy (ergs)	Identification
960707	616/1	50271.419483	5400	2.33(7)	3.0(2)	2.07	5.05	1.6E34	EV Lac 1
960720	675/1	50284.483892	30	1.89(20)	0.33(5)	0.94			GRB960720
960726	689/2	50290.495360	100	2.07(18)	1.1(2)	0.74			GRB960726
960806	735/1	50301.266350	40	1.81(19)	0.34(5)	0.62			GRB960806
960813	757/2	50308.952389	3000	2.04(24)	1.8(3)	0.77			EE Mus
960825	820/2	50320.514881	14400	1.74(14)	23.4(2.0)	0.99	2523.34	2.7E40	IGR J17544-2619 1
961005	1075/2	50361.247077	18000	2.03(9)	19.0(1.3)	1.53	27.57	2.4E36	Algol 1
961229a	1448/2	50446.555400	80	0.79(36)	0.3(2)	1.00			GRB961229a
961229b	1448/1	50446.726181	380	1.70(25)	1.7(3)	0.60			GRB961229b
970111a	1485/2	50459.405560	70	0.65(7)	7.2(4)	0.71			GRB970111
970111b	1487/1	50459.983632	2800	1.50(6)	10.9(5)	1.10			GRB970111b
970123	1565/2	50471.857736	5400	2.16(10)	4.3(3)	1.34	16.56	1.7E35	BY Dra 1
970228	1671/1	50507.123620	75	1.61(8)	3.5(3)	0.86	$z=0.695$	3.6E51	GRB970228
970321	1780/1	50528.194202	5400	2.35(11)	3.5(2)	1.26	15.55	1.2E35	NLTT 51688
970402	1830/1	50540.929040	130	1.06(10)	1.6(2)	0.67			GRB970402
970427a	1930/2	50565.015468	72000	2.37(20)	4.6(6)	4.68	412.39	1.4E38	V969 Mon
970508	1984/2	50576.904010	20	1.75(9)	0.65(5)	0.56	$Z=0.835$	1.0E51	GRB970508
971010	2622/2	50731.675460	3000	2.48(35)	1.6(4)	1.36	10.70	2.4E34	AT Mic
971018	2699/2	50739.377130	10800	2.66(27)	2.4(4)	0.92	14.85	1.0E35	AB Dor 1
971019a	2705/2	50740.664495	23	1.21(15)	1.6(3)	1.09			XRF971019a
971019b	2706/1	50740.738210	200	1.76(28)	0.39(9)	0.84			GRB971019b
971024	2732/1	50745.783860	35	1.68(12)	0.41(4)	0.89			GRB971024
971206a	3066/2	50788.206717	108000	1.99(13)	14.0(1.3)	1.12	98.37	3.5E37	IM Peg
971206b	3066/1	50788.805960	60	1.35(27)	0.7(2)	0.58			GRB971226
971214	3123/1	50796.972640	80	0.62(25)	1.2(3)	0.48	$z=3.418$	3.0E52	GRB971214
971227	3205/2	50809.349380	6	0.46(19)	0.39(7)	0.62			GRB971227
980109	3289/2	50822.050240	50	1.11(12)	1.11(11)	0.91			GRB980109
980128	3465/2	50841.039070	130	1.26(15)	0.50(6)	0.78			GRB980128
980218	3714/1	50862.752755	7200	2.27(39)	2.9(1.1)	0.53	14.85	1.1E35	AB Dor 2
980306	3875/2	50878.161680	70	2.15(21)	0.17(3)	0.48			GRB980306
980311	3905/2	50883.855408	10800	3.08(97)	7.5(7.5)	1.39	2469.14	9.2E39	SAX J1818.6-1703
980326	4057/1	50898.888130	8	1.07(20)	0.7(2)	1.23	$z=0.9$	1.1E51	GRB980326
980329	4073/2	50901.155986	30	0.69(13)	4.3(6)	1.12	$z=3.6$	1.2E53	GRB980329
980412	4169/2	50915.295220	300	1.92(41)	0.34(12)	0.56	408.11	6.9E36	GRB980412
980415	4202/2	50918.645360	100	1.08(37)	0.30(13)	1.20			GRB980415
980415b	4202/2	50918.711636	50400	2.33(8)	9.8(5)	2.11	138.89	3.3E37	GR Dra 1
980425	4281/2	50928.909146	50	1.52(17)	2.3(3)	0.82	$z=0.0085$	3.5E47	GRB980425
980429	4320/2	50932.365567	180	1.84(9)	2.6(2)	1.39			GRB980429
980515	4462/2	50948.708330	50	0.97(16)	1.3(2)	0.94			GRB980515
980519	4480/2	50952.512950	270	1.65(3)	4.9(2)	0.71	$Z=1.58$	2.6E52	GRB980519
980613	4677/2	50977.202150	40	1.57(24)	0.29(6)	1.06	$Z=1.0969$	7.4E50	GRB980613
980614	4683/1	50978.359200	350	0.94(40)	1.1(6)	0.66			GRB980614
980706	4894/2	51000.410380	50	0.97(16)	1.3(2)	0.82			GRB980706
980804	5072/2	51029.678414	50400	1.78(7)	14.3(5)	1.20	50.55	6.2E36	UX Ari
980824	5166/2	51049.607200	60	2.43(39)	0.12(3)	1.05			GRB980824
980907	5275/1	51063.014660	1200	1.33(21)	2.1(4)	0.60	10.89	3.3E34	NLTT18592
980924	5385/1	51080.359688	3000	2.24(25)	1.8(3)	0.81	16.56	5.8E34	BY Dra 2
981018	5618/2	51104.018940	420	1.59(14)	3.3(4)	0.80			GRB981018
981102	5745/1	51119.770233	28800	2.75(38)	2.7(8)	1.03	14.85	1.5E35	AB Dor 3
981217	6002/2	51164.079960	160	1.21(9)	2.0(2)	0.82			GRB981217
981226	6055/1	51173.407872	250	1.86(9)	1.13(7)	0.45	$z=1.11$	2.9E51	GRB981226
981227	6069/2	51174.430038	3000	1.73(11)	2.5(2)	1.21	109.27	5.2E36	V1373 Cen
990123	6221/1	51201.407801	80	0.86(2)	13.0(3)	1.39	$z=1.6$	7.1E52	GRB990123
990125	6231/2	51203.466428	21600	2.30(8)	6.6(3)	0.80	27.57	1.3E36	Algol 2
990217	6383/2	51226.224560	100	1.79(14)	0.43(4)	0.86			GRB990217
990220a	6419/1	51229.584397	10800	6.28(2)	1.0(8)	1.73	5910.17	8.5E39	SAX J1819.3-2525 3
990220b	6419/1	51229.728314	720	1.36(20)	3.6(6)	1.10	2523.34	2.8E39	IGR J17544-2619 2
990227	6473/2	51236.778419	18000	1.77(11)	10.1(6)	0.88	138.89	3.1E37	GR Dra 2
990311	6570/1	51248.754346	2400	2.53(48)	1.3(1.3)	0.38	2523.34	1.0E39	IGR J17544-2619 6
990328	6742/1	51265.715390	250	1.79(29)	0.32(7)	0.93			GRB990328
990413	6829/2	51281.232400	840	1.01(15)	1.6(2)	0.42			GRB990413
990510	6902/2	51308.367450	120	1.36(6)	6.6(3)	0.95	$z=1.6187$	3.7E52	GRB990510
990520	6952/1	51318.085320	15	1.56(17)	0.31(4)	0.54			GRB990520
990526	6975/1	51324.515180	40	2.56(32)	0.19(3)	1.28			GRB990526
990531	6990/1	51329.665601	1800	1.81(15)	4.2(5)	0.97	49.67	1.5E36	CD-33 7795

Table 2. continued.

ID	OP/ WFC	MJD-start	Time span (s)	Photon index	2-30 keV fluence (10^{-6} erg cm $^{-2}$)	χ^2_r	Distance (pc/z)	2-30 keV energy (ergs)	Identification
990625	7072/2	51354.016980	20	1.68(17)	0.60(8)	0.98			GRB990625
990626	7088/2	51355.664400	2400	1.87(10)	5.4(4)	0.93	6.18	2.5E34	EQ Peg
990627	7096/2	51356.208940	40	1.14(12)	0.43(4)	0.78			GRB990627
990704	7141/1	51363.729230	30	1.57(6)	3.2(2)	1.32			GRB990704
990705	7147/2	51364.667650	50	0.88(7)	8.0(6)	1.47	$z=0.843$	1.2E52	GRB990705
990709	7167/1	51368.803083	11880	1.77(19)	3.7(6)	1.13	39.12	1.2E36	II Peg
990712	7188/2	51371.696550	40	1.79(4)	5.1(2)	1.51	$z=0.433$	2.1E51	GRB990712
990722	7263/2	51381.388974	50400	4.16(1.91)	0.6(6)	0.88	39.12	1.3E35	II Peg
990806	7348/1	51396.602860	35	1.43(12)	0.8(1)	0.67			GRB990806
990810	7362/2	51400.612230	1200	1.67(13)	2.4(2)	1.36	44.01	5.8E35	SAX J0346.6-3906
990907	7523/2	51428.732694	190	1.03(10)	2.1(2)	1.06			GRB990907
990908	7523/2	51429.012500	130	1.62(4)	2.6(2)	1.29			GRB990908
990909	7546/2	51430.894314	28800	1.77(6)	82.7(2.1)	1.07	5910.17	5.5E41	SAX J1819.3-2525 2
990911	7553/1	51432.115942	28800	1.49(15)	21.2(2.0)	0.87	2523.34	3.3E40	IGR J17544-2619 3
991005	7692/2	51456.046632	9000	2.12(24)	4.4(7)	0.93	14.85	1.8E35	AB Dor 4
991014	7749/2	51465.911500	7	0.54(23)	0.43(11)	0.63			GRB991014
991026	7820/2	51477.543218	95	1.43(6)	2.7(2)	1.34			GRB991026
991030	7840/2	51481.073224	120	1.16(13)	1.8(2)	0.66			GRB991030
991105	7859/2	51487.694930	100	1.37(13)	1.4(2)	0.90			GRB991105
991106	7860/1	51488.454310	25	1.57(21)	0.19(3)	0.86			GRB991106
991217	8073/2	51529.174610	100	1.59(10)	0.70(6)	1.22			GRB991217
000206	8374/1	51580.866460	40	1.72(9)	0.59(4)	0.55			GRB000206
000208	8386/1	51582.181430	60	1.77(22)	0.25(4)	0.56			GRB000208
000210	8406/1	51584.363870	30	0.91(7)	4.9(3)	0.80	$z=0.8456$	7.5E51	GRB000210
000214	8425/1	51588.042360	100	1.87(7)	1.8(1)	1.00	$z=0.46$	8.2E50	GRB000214
000218	8468/2	51592.667380	505	1.71(11)	3.5(3)	0.56			GRB000218
000312	8683/2	51615.495490	2400	2.13(16)	1.8(2)	0.92	11.70	3.2E34	CD-35 2213
000409	8881/1	51643.237951	3600	2.10(21)	2.1(3)	1.12	14.85	9.1E34	AB Dor 5
000416	8942/2	51650.606060	50	2.21(12)	1.0(1)	0.84			GRB000416
000424	9004/2	51658.762510	20	1.04(14)	0.80(11)	0.87			GRB000424
000528	9145/2	51692.365500	110	0.55(4)	4.5(2)	2.39			GRB000528
000529	9153/2	51693.363410	30	1.46(24)	0.31(6)	0.98			GRB000529
000608	9232/2	51703.368920	50	2.35(25)	0.32(5)	0.81			GRB000608
000615	9251/1	51710.262360	100	1.84(12)	2.2(2)	0.90			GRB000615
000619	9275/1	51714.359805	54000	1.73(7)	18.1(1.0)	0.84	87.53	2.5E37	CF Tuc
000620	9275/2	51715.231620	21	1.01(26)	1.0(2)	1.36			GRB000620
000627	9331/1	51722.501215	2400	2.16(13)	1.6(2)	1.63	5.05	5.2E33	EV Lac 2
000628	9341/2	51723.772880	60	1.45(19)	0.75(12)	0.56			GRB000628
000630	9352/1	51725.281240	70	1.84(17)	0.83(11)	0.93			GRB000630
000901	9696/2	51788.053540	70	0.51(51)	0.8(0.8)	1.14	28.77	8.1E34	GRB000901 [‡]
000920	9832/2	51807.316978	36000	4.19(70)	10.8(10.8)	1.82	2523.34	1.2E40	IGR J17544-2619 4
001008	9934/2	51825.121897	2000	2.00(31)	3.1(1.2)	1.19	2523.34	2.4E39	IGR J17544-2619 5
001011	9957/2	51828.663070	60	1.28(5)	2.1(1)	0.93			GRB001011
001024	10050/1	51841.331705	10	1.30(28)	0.16(4)	1.22			GRB001024
001028	10055/2	51845.510840	120	0.94(48)	0.24(17)	0.79			GRB001028
001101	10091/1	51849.790690	150	2.39(16)	0.59(6)	0.91			GRB001101
001109	10146/1	51857.391080	65	1.22(8)	1.89(14)	0.95			GRB001109
001110	10159/2	51858.592130	60	1.40(16)	0.84(11)	0.62			GRB001110
001207	10302/1	51885.179691	2400	2.11(4)	6.5(2)	3.61	11.55	1.4E35	CC Eri
001213	10320/2	51891.353117	12600	1.71(13)	6.6(7)	1.25	42.51	2.9E36	AR Lac 1
010119	10570/1	51927.832386	86400	2.19(10)	9.7(6)	1.44	27.57	2.1E36	Algol 3
010213	10725/2	51953.123154	25	1.01(9)	2.0(2)	0.91			GRB010213
010214	10727/2	51954.366670	40	0.95(11)	0.88(8)	0.67			GRB010214
010219	10747/1	51959.258830	30	2.18(17)	0.90(10)	0.80			GRB010219
010220	10753/2	51960.952140	200	0.79(10)	1.80(15)	1.46			GRB010220
010222	10767/1	51962.306539	200	1.49(3)	24.3(5)	2.34	$z=1.477$	1.1E53	GRB010222
010301	10800/1	51969.647174	2400	2.39(14)	4.4(3)	1.60	14.85	1.3E35	AB Dor 6
010304	10822/2	51972.221390	20	0.70(8)	1.71(13)	1.07			GRB010324
010304b	10822/1	51972.42479	50400	2.33(68)	3.5(3.5)	2.12			IGR J08408-4503
010315	10883/1	51981.336717	234000	1.97(5)	47.2(1.1)	3.09	119.09	2.1E38	GT Mus
010320	10923/1	51988.863100	31	1.13(20)	0.71(13)	1.49			GRB010320
010324a	10954/1	51992.480173	400	1.42(15)	7.8(9)	1.36			GRB010324
010324b	10954/2	51992.622915	3300	2.49(42)	1.9(1.4)	1.41	6097.56	9.2E39	AX J1845.0-0433
010327	10972/1	51995.627257	10800	2.57(34)	2.0(5)	0.97	14.85	8.1E34	AB Dor 7
010412	11085/1	52011.907276	100	1.16(6)	4.9(2)	0.89			GRB010412
010501a	11203/2	52030.080697	200	1.19(14)	0.64(7)	1.36			GRB010501A

Table 2. continued.

ID	OP/ WFC	MJD-start	Time span (s)	Photon index	2-30 keV fluence (10 ⁻⁶ erg cm ⁻²)	χ^2_r	Distance (pc/z)	2-30 keV energy (ergs)	Identification
010501B	11203/1	52030.276181	40	0.19(25)	0.52(14)	0.63			GRB010501B
010512	11268/1	52041.029624	3600	2.16(27)	1.8(4)	1.37	42.51	5.3E35	AR Lac 2
010518	11292/2	52047.278780	300	1.25(23)	0.93(20)	1.22			GRB010518
010527	11324/2	52056.347470	90	1.75(21)	1.0(2)	1.26			GRB010527
010528	11330/1	52057.734213	2100	2.04(15)	2.5(3)	0.92	10.76	3.7E34	V857 Cen
010707	11486/1	52097.287850	20	1.83(12)	0.30(2)	2.09			GRB010707
010824	11828/2	52145.123067	1500	1.71(2.11)	0.2(2)	1.02	44.01	5.1E34	SAX J0346-3906
011030	12150/1	52212.268328	350	1.72(10)	1.1(1)	1.02			GRB011030
011103	12167/2	52216.139073	5400	2.08(22)	2.8(5)	1.02	42.51	8.1E35	AR Lac 3
011121	12252/1	52234.782435	100	1.36(3)	14.6(4)	1.06	z=0.36	4.0E51	GRB011121
011211	12361/1	52254.795040	400	1.43(7)	2.7(2)	0.88	z=2.1435	2.6E52	GRB011211
020113	12497/2	52287.887420	800	1.59(20)	0.63(11)	1.67			GRB020113
020118	12513/2	52292.769646	60	1.36(15)	1.2(2)	0.59			GRB020118
020321	12705/1	52354.180980	60	0.99(24)	0.31(7)	0.91			GRB020321
020322	12712/2	52355.160819	60	1.40(14)	0.65(7)	0.80	z=1.80	4.5E51	GRB020322
020409	12830/1	52373.882928	50	1.26(23)	1.00(22)	0.56			GRB020409
020410	12830/2	52374.444190	1300	1.80(4)	9.6(3)	1.01			GRB020410
020427	12933/2	52391.158813	70	2.11(14)	0.62(6)	0.43	z=2.30	7.0E51	GRB020427

[‡]For GRB000901, the distance and energy output were applied for an identification with EQ J084834.9-785352. See Table 1.